SANDIA REPORT
SAND2012-8198
Unlimited Release
September 2012

Detectability of Neuronal Currents in Human Brain with Magnetic Resonance Spectroscopy

Howland D. T. Jones, Andrew R. Mayer, Arvind Caprihan, David M. Haaland, Edward V. Thomas, Charles Gasparovic, Jason C. Harper, Krastan B. Blagoev

Prepared by
Sandia National Laboratories
Albuquerque, New Mexico 87185 and Livermore, California 94550

Sandia National Laboratories is a multi-program laboratory managed and operated by Sandia Corporation, a wholly owned subsidiary of Lockheed Martin Corporation, for the U.S. Department of Energy's National Nuclear Security Administration under contract DE-AC04-94AL85000.

Issued by Sandia National Laboratories, operated for the United States Department of Energy by Sandia Corporation.

Available to DOE and DOE contractors from
U.S. Department of Energy
Office of Scientific and Technical Information
P.O. Box 62
Oak Ridge, TN 37831

Telephone: (865) 576-8401
Facsimile: (865) 576-5728
E-Mail: reports@adonis.osti.gov
Online ordering: http://www.osti.gov/bridge

Available to the public from
U.S. Department of Commerce
National Technical Information Service
5285 Port Royal Rd.
Springfield, VA 22161

Telephone: (800) 553-6847
Facsimile: (703) 605-6900
E-Mail: orders@ntis.fedworld.gov
Online order: http://www.ntis.gov/help/ordermethods.asp?loc=7-4-0#online

SAND2012-8198
Unlimited Release
September 2012

Detectability of Neuronal Currents in Human Brain with Magnetic Resonance Spectroscopy

Howland D. T. Jones[1], Andrew R. Mayer[2,3], Arvind Caprihan[2], David M. Haaland[1], Edward V. Thomas[1], Charles Gasparovic[2,3], Jason C. Harper[1], Krastan B. Blagoev[2,4]

[1]Sandia National Laboratories, MS 0895, Albuquerque, NM 87185-0895,
[2]The Mind Research Network, Albuquerque, NM 87131, USA
[3]Department of Neurology, University of New Mexico, Albuquerque, NM 87131, USA
[4]Theoretical Division, Los Alamos National Laboratory, Los Alamos, NM 87544, USA

Abstract

Magnetic resonance spectroscopy has been used in a high-risk, high-payoff search for neuronal current (NC) signals in the free induction decay (FID) data from the visual cortex of human subjects during visual stimulation. If successful, this approach could make possible the detection of neuronal currents in the brain at high spatial and temporal resolution. Our initial experiments indicated the presence of a statistically significant change in the FID containing the NC relative to FIDs with the NC absent, and this signal was consistent with the presence of NC. Unfortunately, two follow-on experiments were not able to confirm or replicate the positive findings of the first experiment. However, even if the result from the first experiment were evidence of NC in the FID, it is clear that its effect is so small, that a true NC imaging experiment would not be possible with the current instrumentation and experimental protocol used here.

CONTENTS

FIGURES

TABLES

NOMENCLATURE

AFNI	analysis of Functional NeuroImages
ANOVA	analysis of variance
BOLD	blood oxygenation level dependent
CART	classification and regression trees
EEG	electroencephalography
ERC	event-related neuronal currents
FID	free-induction decay
fMRI	functional magnetic resonance imaging
MEG	magnetoencephalography
MCR	multivariate curve resolution
MRI	magnetic resonance imaging
NC	neuronal currents
ncMRI	neuronal current magnetic resonance imaging
PCA	principal components analysis
PLS	partial least squares
PRESS	point-resolved spectroscopy
SPM	statistical parametric map

1. INTRODUCTION

A magnetic resonance system capable of imaging neuronal current distribution would be of great utility to neuroscience and medicine by allowing researchers or clinicians to map the changes in the neuronal dynamics associated with a given stimulus at both high spatial and temporal resolution. Electroencephalography (EEG) and magnetoencephalography (MEG) measure the electro-magnetic fields generated outside the scalp and can estimate the location and size of an equivalent current dipole in the brain by inverse modeling (Hamalainen *et al.*, 1993). These methods have high temporal resolution but the spatial location suffers from the difficulties of ill-posed inverse problems. Functional magnetic resonance imaging (fMRI) based on blood oxygenation level dependent (BOLD) response (Ogawa *et al.*, 1990) provides a high resolution image of the change in hemodynamic response to the neuronal activity, but has poor temporal resolution. fMRI measurement depends in a complex way on the change in blood oxygenation level, a change in cerebral blood flow, and a change in cerebral blood volume. The BOLD response is not a simple measure of the hemodynamic response nor is it a direct measure of neuronal current in the brain. The neuronal activity creates the energetic demands which results in the hemodynamic response. This effect is known as neurovascular coupling, and the basis of the hemodynamic response has been discussed by Logothetis (Logothetis, 2008). A recent paper has demonstrated that in certain situations the hemodynamic response can anticipate the neuronal activity (Sirotin and Das, 2009). Event-related neuronal currents (ERC) that give rise to the MEG signal are also expected to induce magnetic field changes inside the brain close to the neuronal activity, which in theory, could be measured with magnetic resonance techniques. A successful development of neuronal current magnetic resonance imaging (ncMRI) to image these ERCs or neuronal currents (NC) would allow the direct measure of neuronal activity with the high spatial resolution of magnetic resonance imaging (MRI) and the high temporal resolution of MEG and would be very useful new tool in many neuroscience studies.

There have not been convincing reproducible experiments demonstrating ncMRI. The efforts in measuring neuronal current by MRI have been reviewed by Bandetinni *et al.* (Bandettini *et al.*, 2005) and the challenges of detecting neuronal currents by MRI were discussed by Hagberg *et al.* (Hagberg *et al.*, 2006). Rather than repeat the discussion in these papers, we complement the previous reviews with a discussion on studies completed since 2006 and give importance to the care that has to be taken to detect neuronal currents by MRI. We begin by pointing out some differences between fMRI and ncMRI. Both the BOLD response in fMRI and the neuronal currents change the local magnetic field properties. The BOLD response changes the local magnetic susceptibility which in turn changes the local magnetic field, while a neuronal current will directly change the local magnetic field. The BOLD contrast is stronger at higher fields because the change in the magnetic field is proportional to the product of the change in susceptibility and the main magnetic field B0, while the neuronal currents will generate a magnetic field which does not depend on the main magnetic field B0. In principle lower fields may offer better ncMRI detection because the ncMRI will be the same at lower fields while the BOLD response will be weaker, making it easier to separate the two effects. The BOLD hemodynamic response is temporally slow. It starts within 1-2 s after the stimulus and can last more than 20 s for stimulation times of a few seconds or less. The far-field neuronal current response as measured by MEG on the scalp is a transient; it lasts for about 300 ms and

has asymmetric biphasic temporal pattern with a peak at about 100 ms after the stimulus, the exact value depending on the stimulus (Hamalainen et al., 1993). The results of a MEG experiment in our lab with a visual stimulus similar to the one used in the fMRI experiment is shown in Figure 1. It has a peak at around 120 ms after the stimulus, and its duration is 300 ms. It is not clear whether the near-field response of the neuronal activity, as measured by MRI, will be similar to the far-field response. Direct measurement of neuronal activity by microelectrodes placed directly in the brain has shown responses in the range of kHz (Logothetis, 2002).

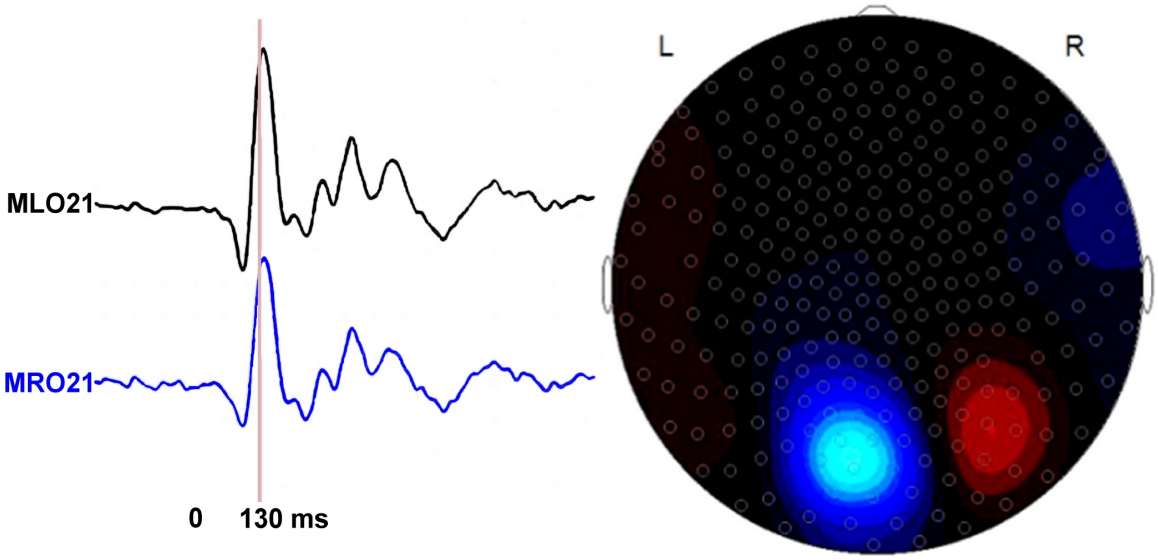

Figure 1. MEG responses to visual stimulation and the resulting MEG image of a human subject.

Kraus *et al*. (Kraus *et al.*, 2008) have proposed low-field experiments based on the possible resonant mechanisms that arise when the Larmor resonant frequency of magnetic resonance at low fields matches the neuronal activity oscillations frequency (less than ~2 KHz) (Logothetis, 2002). In these experiments the neuronal activity is taken as the B1 magnetic field for excitation. These experiments could not be performed at higher fields because the magnetic resonance frequency would be in the MHz range. A stimulus rotary saturation method has been proposed recently which effectively lowers the Larmor frequency in a high-field system to the order of 100 Hz based on the spin-locking mechanism (Witzel *et al.*, 2008). In phantom experiments this method had the sensitivity to detect magnetic fields generated by current dipoles similar in magnitude and frequency to that detected by MEG.

In an MRI experiment only perturbations to the magnetic field parallel to the main magnetic field can be detected. This means that a current parallel to the main magnetic field, which generates magnetic fields perpendicular to the main magnetic field, cannot be detected by MRI. In addition, if we collect data from a single voxel, the phase of the signal in the voxel depends on the mean magnetic field within that voxel and the signal attenuation depends on magnetic field homogeneity within the voxel (Konn *et al.*, 2003). The MRI signal attenuation can be modeled in terms of the variance of the magnetic-field distribution in the voxel, with

higher variance implying greater attenuation. The general consensus has been that because of the spatial symmetry of the magnetic field generated by a current dipole, the mean field in a voxel centered on the activity will be zero and no phase effects will be observed, while off-center voxels will show phase effects. The magnitude attenuation will be largest in the voxel with the neuronal activity (Konn *et al.*, 2003). In an imaging experiment with small voxel sizes, the signal magnitude may be more sensitive to neuronal activity if it includes the neuronal current source, while the signal phase may be more sensitive if it is an off-center voxel. In addition, for BOLD fMRI the phase signal has been shown to be more sensitive to physiological noise (respiration) (Hagberg *et al.*, 2008) and almost all fMRI is based on magnitude signal changes only.

The first attempt to measure neuronal activity by MRI was completed in 1994 (Singh, 1994). The study was interesting because it built a current phantom, calibrated the current to the magnetic fields measured by MEG at the scalp, used a spin-echo experiment to rectify the phase loss caused by the biphasic nature of the neuronal response, and performed an actual MRI experiment in a subject. The experiment was unsuccessful but the phantom study showed that an equivalent MEG sensitivity would require one to detect 0.35 degrees phase change from the neuronal current while with technology available at that time Singh could only detect 6.8 degrees of phase shift. ncMRI studies actively started after 1999 (Bodurka *et al.*, 1999; Kamei *et al.,* 1999) and are reviewed in (Bandettini *et al.*, 2005). Theoretical modeling and computer simulations modeled current dipoles (Heller *et al.*, 2009; Konn *et al.*, 2003) and more recently models of dendrites and axons were made (Blagoev *et al.*, 2007; Cassara *et al.*, 2008; Luo *et al.*, 2011a; Park and Lee, 2007; Xue *et al.*, 2006). The expected magnitude change from the neuronal current ranges from 2% (Xue *et al.*, 2006) to 10^{-6} % (Park and Lee, 2007) and the phase change ranges from 9.7 degrees (Xue *et al.*, 2006) to 0.0004 degrees (Heller *et al.*, 2009). Except for the simulation results of (Blagoev *et al.*, 2007; Xue *et al.*, 2006), the other simulations suggest that neuronal currents cannot be detected by current MRI technology. In a BOLD fMRI experiment, it is easy to detect a 2% magnitude change and 1 degree phase change (Feng *et al.*, 2009).

In order to get stronger neuronal effects, several studies have tried to detect neuronal activity in epilepsy subjects (Liston *et al.*, 2004; Rodionov *et al.*, 2010; Sundaram *et al.*, 2010). The equivalent current-dipole is expected to be an order of magnitude stronger than that expected from stimulus experiments. Simultaneous EEG/fMRI experiments (Rodionov *et al.*, 2010) were performed to enable synchronization of MRI experiments to neuronal activity. Fast-response MRI signals were detected by MRI, but the experiment could not confidently attribute the detected signals to neuronal activity rather than BOLD related response to internal epileptic discharges. In a separate EEG/fMRI study (Sundaram *et al.*, 2010), both phase and magnitude changes were observed in fast-response MRI signal which could be attributed to epileptic discharges. The study of epileptic subjects with joint EEG/fMRI experiments appears to be useful in mapping the neuronal current response by MRI. A number of following factors make it difficult to detect neuronal activity by MRI:

a) **Location.** A BOLD experiment can be done to localize the region where neuronal activity will be measured. Experiments of (Kim *et al.*, 2004; Logothetis *et al.*, 2001) have shown that the BOLD activity and neuronal activity are in close spatial proximity, and with voxel sizes larger than 2x2x2 mm, the BOLD voxel will also contain the neuronal activity location. One problem is that the presence of large veins can change the location of BOLD activity downstream from that of neuronal activity.

b) **Capturing the transient neuronal activity**. If we assume that the near-field neuronal response to be measured by MRI is similar to the far-field neuronal response measured by MEG, then for an MRI imaging experiment, the zero phase-encoding echo should correspond to the peak of neuronal activity. The situation is slightly different for the single-voxel spectroscopy experiment we describe here. In this case, as discussed in the Appendix, depending on the location of the stimulus with respect to the spin-echo, the neuronal currents can affect the entire spin-echo. If this effect were strong, then it could be used to measure the time evolution of neuronal currents. If the neuronal current time response was known, then some optimization can be done to define its origin with respect to the MR experiment to maximize its effect on the spin-echo. In conclusion, a careful synchronization between the expected time of the neuronal response and the MR imaging experiment is required.

c) **Suppressing the BOLD response**. Because the BOLD response and neuronal activity response will occur in the same voxel, these signals have to be separated because of their different temporal characteristics. While the neuronal response occurs immediately after the stimulus, the BOLD response is slower and starts with an approximate delay of 1-2 s after the stimulus. The problem in any periodic experiment is that the BOLD response from the previous stimulus could interfere with the neuronal response of the next stimulus. If the stimuli are applied with a repetition time of approximately 30 s, then the BOLD response from the previous stimulus will have completely died down and the response to the next stimulus will be free from the BOLD response for approximately the first 2 seconds after the next stimulus response. This approach is expected to separate the neuronal current response from the BOLD response and has been applied to detect neuronal activity in an imaging experiment without success (Luo *et al.*, 2011b). Another method to reduce BOLD contribution is to apply the stimulus rapidly so that the BOLD response is saturated and the neuronal current response would be riding on a relatively constant BOLD signal. A success was reported by this method of BOLD suppression by (Xiong *et al.*, 2003). Several other research groups have tried detecting neuronal currents by suppressing the BOLD signal by saturation without reporting success (Chu *et al.*, 2004; Parkes *et al.*, 2007; Tang *et al.*, 2008). Neuronal current response has been successfully measured in snail ganglia as a decrease in signal magnitude (Luo *et al.*, 2009; Park *et al.*, 2006). Snail ganglia transport oxygen bound to non-magnetic hemocyanin, in contrast to magnetic hemoglobin, and the BOLD response is absent in these snail experiments. Conceptually a similar study in bloodless turtle brain did not report detecting neuronal activity by MRI (Luo *et al.*, 2009).

d) **Physiological noise**. The signal change because of physiological factors such as respiration and cardiac cycle can be larger than the expected neuronal current response (Hagberg *et al.*, 2008; Hagberg *et al.*, 2006). These effects are in addition to the problems of subject motion and the subject being startled with the sudden application of the stimulus. Respiration and the cardiac cycle can be monitored. The respiration affects the phase signal more than magnitude signal and consequently almost all the BOLD fMRI studies are based on the magnitude signal.

The MRI experiment can be performed either as an imaging experiment where each slice is imaged in about 80 ms or a single voxel experiment where the data are collected immediately

after the stimulus and the temporal resolution is limited by the sampling rate. The imaging experiment has the advantage that a spatial resolution of 2x2x2 mm is achievable with a 3T magnet while the single voxel experiment will have a larger voxel size of the order of 10x10x10 mm. A single voxel BOLD response was seen in 1994 (Hennig *et al.*, 1994). Hennig *et al.* called their method oxygenation sensitive functional spectrocopy and here we will refer to it as fMRS (functional magnetic resonance spectroscopy). Because of voxel selection these are spin-echo experiments, and one typically collects one-half of the spin-echo after the voxel has been selected. The resulting signal is not strictly the free-induction decay (FID) signal, but we will call it such in this paper. The single voxel experiment has the advantage that the response of the neuronal activity can be synchronized with any part of the FID. The single voxel experiment can experience a partial-volume dimunization of the signal because the region of neuronal activity might be much smaller than the voxel size. An additional problem occurs if the voxel is placed in error or if the subject moves since the region of neoronal activity may no longer lie within the selected voxel.

In this study we report results based on single-voxel fMRS studies originally designed to demonstrate the potential feasibility of some future neuronal current MR imaging technique. We employed two BOLD suppression methods in this work. In several of our experiments, we used long repetition time of the stimulus so that the MRI signal observed after the stimulus is free from the BOLD signal. A similar experiment in parallel has been done in a imaging context with negative findings for detecting neuronal activity (Luo *et al.*, 2011b). In another experiment, we attempted to saturate the BOLD signal with a relatively rapid application of the stimuli.

In an MR imaging experiment the magnitude and the phase at any image voxel is heavily weighted by the magnetic field properties (variance and mean of the magnetic-field distribution) at the zero phase-encoding step. The time duration of the magnetic field transient caused by neuronal currents (~100 ms) is of the same order as the time taken to obtain the image. Thus with careful synchronization, one could align the strongest neuronal-current magnetic field change to the zero phase-encoding steps. Even if this synchronization could be successfully accomplished, it is not clear how the biphasic nature of the neuronal current response will interact with an MRI signal.

In this investigation, we take a fundamentally different approach from past ncMRI studies by collecting half of the spin-echo (termed the FID) of the water signal from the visual cortex soon after visual stimulation (see Appendix). The beginning of the FID acquisition is timed to coincide with the putative neuronal current response. Hence, if the neuronal current response were sufficiently strong, we would observe changes in the attenuation and phase of the FID during its decay. The collection of the entire FID gives us the flexibility to analyze its time course in an optimal manner. We also describe studies to better understand the detrimental effects of instrument drift and physiological drift caused by respiration and heart beat and to understand the optimal methods to prepare the data for analysis. We apply a variety of multivariate and statistical analysis methods in the search of evidence of the influence of neuronal current as it subtly changes the decay of the FIDs collected during these experiments. This paper details the procedures used, the analysis methods employed, and discusses the results of these experiments designed to detect the presence of neuronal currents in the MRS data.

2. METHODS

2.1. Human Subjects Experiment 1

2.1.1. Subjects

Ten adult volunteers (3 men; mean subject age = 27.4 +/- 8.4 years) were included in the first experiment. None of the study participants were taking psychoactive prescriptive medications or had a history of neurological, psychiatric or substance abuse disorders. Informed consent was obtained from all subjects according to institutional guidelines at the University of New Mexico with concurring approvals from Sandia National Laboratories.

2.1.2. Timing of Stimulus Delivery

Timing was crucial in the current experiment given the short duration of useful signal during the free induction decay (~250 ms). We therefore conducted several hundred measurements to obtain the exact timing of visual stimulus delivery for the MR presentation system to account for delays in both computers and projectors. Specifically, we measured the time differences from when a pulse was sent out from the scanner to trigger the delivery of the visual stimulus to when a visual stimulus was actually recorded from the projector using a phototransistor diode. The Presentation software program and a PowerLab Data Acquisition System were used to present visual stimuli and a phototransistor with a response time of 2 nanoseconds was used to measure actual stimulus onset times. Results indicated a mean delay of 41 ms in stimulus presentation times with a jitter (one standard deviation) of 3.6 ms compared to the onset of the MR trigger. This delay was then used in conjunction with other image acquisition delays as an offset to maximize the likelihood of the M100 response occurring at 36 ± 6.6 ms into the FID, when signal was likely to be maximal.

Visual stimuli included a central fixation cross and full field, black and white checkerboard that reversed (2 Hz). In addition, a similar reversing red and white checkerboard was also employed as target trials. The fixation cross was also embedded in the checkerboard to facilitate the maintenance of visual fixation throughout the course of the experiment. Subjects were instructed to passively view the visual stimuli, which were rear-projected (Sharp XG-C50X LCD projector) onto a plexiglass screen. A visual, rather than auditory, task was chosen due the acoustic noise generated from the switching of the gradient coils, which has been shown to produce constant BOLD related activity in the primary auditory cortex (Bandettini *et al*., 1998). Moreover, the spatial and temporal dynamics of the initial visual response are well characterized through other neuroimaging modalities (MEG/FMRI/optical imaging). Thus, our results could more readily be compared to these more established measures.

2.1.3. MRI and MRS Data Acquisition

All functional (fMRI and MRS) and structural (high-resolution T1 images) data were collected on a Siemens 3T scanner at The Mind Research Network. A 12-channel headcoil was used for all imaging modalities to maximize signal-to-noise ratios. High-resolution T1-weighted anatomic images were acquired with a 5-echo multi-echo MPRAGE sequence [TE (echo time) =

1.64, 3.5, 5.36, 7.22 and 9.08 ms, TR (repetition time) = 2.53 s, TI (inversion time) = 1.2 s, 7° flip angle, NEX (number of excitations) = 1, slice thickness = 1 mm, FOV (field of view) = 256 mm, resolution = 256 x 256]. The images were subsequently angled along the calcarine fissure at the scanner to best visualize the region of interest in the V1 region of the visual cortex. FMRI experiments were then performed during the presentation of the visual stimulus to better localize the visual cortex based on the BOLD response using a single-shot, gradient-echo echoplanar pulse sequence [TR = 2000 ms; TE = 29 ms; flip angle = 75°**;** FOV = 240 mm; matrix size = 64 x 64]. The first three images of the run were eliminated to account for T1 equilibrium effects. The EPI slices were prescribed to be co-registered with the high-resolution T1 images.

The MRS water proton signal was acquired with a single-voxel point-resolved spectroscopy (PRESS) experiment (flip angle=90°, TR= 3 s, TE=30 ms, bandwidth=1000 Hz, number of points=1024) and modified to deliver a trigger pulse to start the stimulus presentation system to maximize timing efficiency. The transmitter frequency was set to the water resonance frequency before each block of experiments. The dimensions of the voxel were 1 x 2 x 1 cm centered on the region of maximum BOLD signal observed in the fMRI images and anatomical landmarks from the T1 data. The magnetic field homogeneity in the region of the voxel was optimized using automatic adjustments with the transmitter frequency set to the water proton frequency.

The experimental paradigm consisted of several successive stages. During the first stage, high-resolution T1 weighted images were acquired to improve the visualization of anatomical landmarks. During the second stage, a scout EPI image was generated, which was then used to generate a registration matrix from EPI to T1 space. Subjects next passively viewed the reversing checkerboard in a blocked design (10 s of stimulation followed by 16-20 s of rest; 10 cycles) while undergoing BOLD neuroimaging. While the subject rested quietly in the scanner, the resulting BOLD data was analyzed (approximately 2 minutes to execute a batched program) and a statistical parametric map (SPM) was constructed to identify the maximal region of activation within V1. This SPM was then mapped onto the high-resolution anatomical images on a subject-by-subject basis to facilitate the identification of maximal activation in relation to local landmarks (i.e., calcarine fissure). A single voxel was then placed in the region of maximal activation for the measurement of the putative neuronal current.

During the final stage of the experiment, visual stimuli were briefly presented in an event-related design while 1H-MRS data were collected (see Figure 2 for the sequence of FIDs and stimuli and Figure 3 for the design of the entire Experiment 1). Trials randomly consisted of 12 or 13 1H-MRS FIDs with the visual stimuli presented such that the NC would appear during the 6^{th} or 7^{th} FIDs. Specifically, the 2 Hz reversing checkerboard was presented for 3000 ms followed by an inter-trial interval of at least 36 s. For ease of data analysis, the first FID for trials consisting of 13 1H-MRS FIDs was deleted from the data. Therefore, the data set that was analyzed had all trials consisting of 12 FIDs with the NC occurring during the sixth FID. Participants were presented with either a black or a red reversing checkerboard and asked to press a button when a red checkerboard was detected. A long inter-trial interval was selected to allow the BOLD response to completely recover due to uncertainty as to whether the physiological BOLD noise could either be suppressed through rapid presentation or statistically accounted for with deconvolution during the detection of neuronal currents. Although each FID

was 1024 ms long, the signal deteriorated into the noise level after approximately 250 ms of data collection and the first 3 ms appeared to be contaminated by a receiver-gating artifact. Therefore, the first 3 data points were deleted from all FIDs before analyses were performed. An eigenvector analysis of the data, which increases the sensitivity to small signals, confirmed that a small amount of signal persisted to approximately 550 ms.

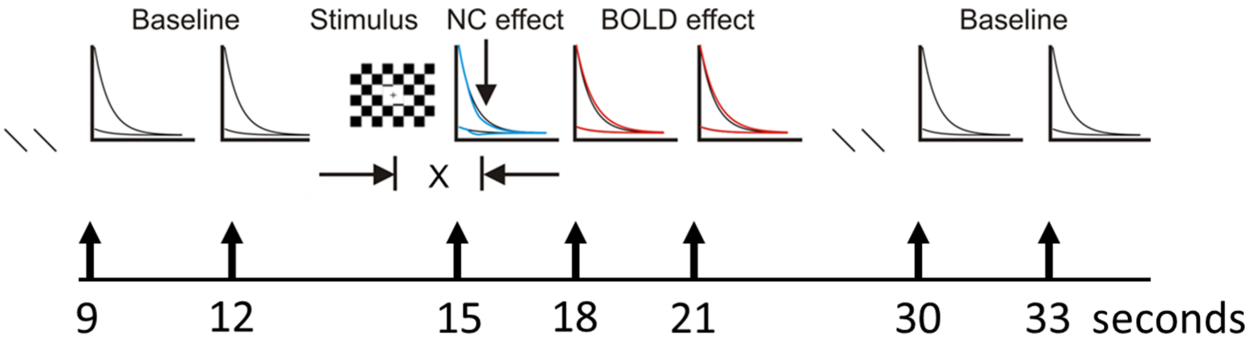

Figure 2. Design of Experiment 1 demonstrating the FIDs and their arrangement relative to the visual stimulation.

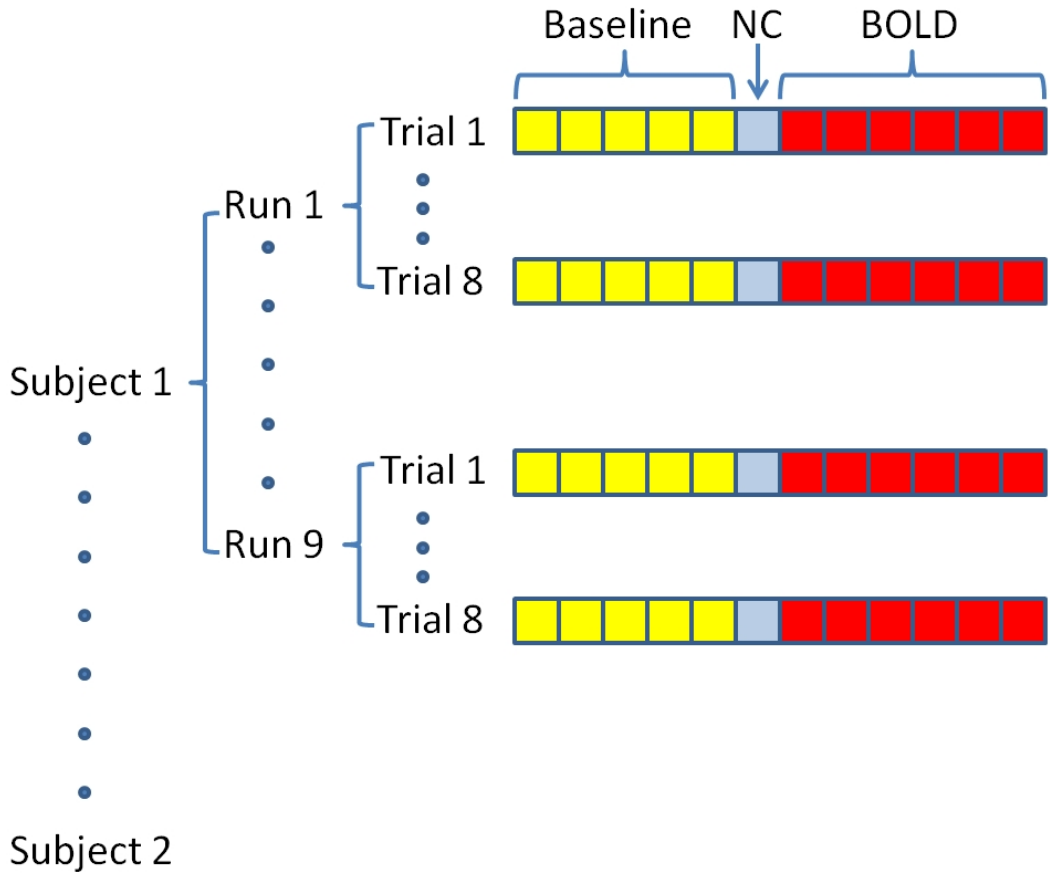

Figure 3. Design of Experiment 1 showing the 12 FIDs per trial with location of the baseline FIDs, FID with NC, and FIDs with BOLD response along with the arrangement of the trial, run, and subject experimental design.

The first five FIDs of each trial served as a baseline measure through which background correction algorithms were implemented. These FIDs were assumed to not be affected by stimulus-induced ERC or BOLD effects (see Results and Discussion Section). The sixth FID corresponded to the putative neuronal current, whereas FIDs 7-11 could be used to measure the effects of the BOLD response. The data were collected in 8 runs separated by intervals of 30-45 s, during which participants were given a chance to rest their eyes. There were a total of 9 trials per run, or 72 total trials in the experiment. Physiological data, including pulse rate and respiration, were collected for all subjects using a respiratory belt transducer and a photoplethysmograph. The final data set that was used in the analyses consisted of 8640 FIDs (10 subjects x 9 runs x 8 trials x 12 FIDs) along with a data file that contained FID number, run number, trial number, heart rate, respiratory rate, subject number, presence (1) or absence (0) of stimulus, and the time (ms) after the start of the FID where the M100 response was expected relative to the photodiode signal indicating the start of the visual stimulation.

2.1.4. fMRI Analysis

Functional images were generated using Analysis of Functional NeuroImages (AFNI) software package (Cox, 1996). Prior to the start of the experiment, an ideal function was generated by convolving a square wave, consisting of the visual stimulation (checkerboard) and rest periods (fixation cross), with a gamma variate function corresponding to the shape of the hemodynamic response (Cohen, 1997). Time series data were then interpolated in time to correct for slice acquisition differences and spatially registered in both 2 and 3-dimensions to minimize effects of head motion. The preprocessed data were then correlated with the ideal function to obtain a SPM of neuronal regions that covaried with stimulus presentation. A parametric threshold was then applied to the SPM map to reduce false positives and localize the task-dependent BOLD response within the visual cortex. The functional data was then overlaid on each individual's high resolution T1 scans to improve the visualization of anatomical landmarks and facilitate subsequent placement of the MRS voxel.

2.2. Human Subjects Experiment 2

Nine adult volunteers (6 men; mean subject age = 31.8 +/- 9.1 years) completed Experiment 2. One subject was repeated in the study so Experiment 2 consisted of a total of 10 subject runs. Several task and imaging parameters were altered in Experiment 2 to further quantify the positive effects that were observed during Experiment 1. Foremost, we attempted to suppress the BOLD effect through saturation (i.e., extremely short inter-trial intervals) in Experiment 2 rather than through extinction (i.e., extremely long inter-trial intervals) as occurred in Experiment 1. An additional benefit of this design should be the reduction in the startle effect associated with infrequently presented sensory stimuli. Finally, in addition to visual stimuli, trials that involved only auditory stimuli were also conducted to further study potential confounds associated with startle. As an additional verification of the neuronal current signature, two different delays were used to determine if measurable differences in the FID could be detected as a result of the delay in stimulus presentation (and associated M100 response). The voxel was placed within the visual cortex for both the auditory and the visual trials. Moreover, several of the imaging parameters were altered to reflect the shortened intervals between stimuli. However, the general order of data collection (high-resolution anatomical images, BOLD-based functional localization and 1H-MRS runs to detect neuronal currents) was identical across the two experiments. Additional details of these alterations are discussed below.

The data acquisition parameters for the high-resolution T1 image and echo-planar imaging were identical between Experiments 1 and 2. The MRS water proton signal was acquired with a single-voxel point-resolved spectroscopy (PRESS) experiment with identical parameters to Experiment 1, with the exceptions of a reduction in the TR (flip angle=90°, TR= 500 ms, TE=30 ms, bandwidth=1000 Hz, number of points=1024).

During the 1H-MRS experiments, auditory or visual stimuli were presented once every 1500 ms. Visual stimuli consisted of either a static black (non-target trials; 66% of trials) or red (target trials; 34% of trials) checkerboard that was presented for 500 ms in contrast to the reversing checkerboard (2 Hz frequency in Experiment 1). Auditory stimuli consisted of either

1000 Hz (non-target; 66% of trials) or 2000 Hz (target; 34% of trials) pure tones of 500 ms duration. A linear ramp in the frequency and amplitude of the auditory stimulus for the first and last 10 ms was used to decrease the likelihood of audible clicks at stimuli onset/offset. In addition, two different delays were used such that the M100 response was predicted to occur at either 20 ms or 50 ms into the FID. Auditory or visual stimuli were presented exclusively within each run, and run order was counter-balanced (ABBA) across each experiment, i.e., the visual and auditory stimuli were blocked within each run.

2.3. Human Subjects Experiment 3

Eleven adult volunteers (8 men; mean subject age = 34.9 +/- 8.2 years) completed Experiment 3. Experiment 3 was a replication attempt of the findings of Experiment 1 with a few key exceptions. Foremost, instead of presenting 72 visual trials, a total of 40 visual and 40 auditory trials were presented across 10 different runs. The auditory trials were incorporated into the experiment as an additional control for the startle effect associated with temporally infrequent stimuli. For all trials, the voxel was placed in the visual cortex. Auditory and visual trials were pseudo-randomized within each run, with the constraint that a total of 5 visual and 5 auditory trials were required to occur within each run to improve the local homogeneity. Similar to the visual stimuli (two different types of reversing checkerboards), the auditory trials consisted of pure tones that alternated at a 2 Hz frequency. Subjects were instructed to press a button when the target stimuli were presented and to not press the button when the non-target stimuli were presented. Specifically, the non-target trials (80% of trials) consisted of alternating 1000 and 2000 Hz tones (duration 500 ms), whereas the target trials (20% of trials) alternated between 2000 and 3000 Hz tones. A linear ramp of 10 ms was applied to the frequency and amplitude of the auditory stimulus to decrease the likelihood of audible clicks at stimuli onset/offset. A delay in stimulus presentation was again used such that the M100 response was predicted to occur at the same time within the FID as Experiment 1. However, in this experiment, the photodiode response was erratic, and it is uncertain if the stimulus was centered at the same time location as in the first experiment. Based upon the photodiode data, the M100 response may have been located 21 ms after that start of the FID. Another difference between Experiment 1 and Experiment 3 was that that the minimal inter-trial interval was increased to 39 seconds to further reduce the likelihood of BOLD contamination. However, similar to Experiment 1 only the first 12 stimuli were used for experimental analyses. Otherwise, all other experimental parameters, imaging parameters and order of data collection (high-resolution anatomical images, BOLD based functional localization and 1H-MRS runs to detect neuronal currents) were identical across the two experiments.

2.4. Agar Phantoms

A 17.5 cm diameter spherical agar phantom with relaxation times T1 and T2 comparable to gray matter at 3T was used in the MRS experiments to optimize the instrumental parameters as well as to monitor the drift characteristics of the instrument in the absence of physiological variations that would be present in human subjects. In these agar phantom studies, we varied the voxel placement in the sphere (center vs. edge), the voxel location (center vs. edge), the voxel

dimensions (1 x 1 x 1 cm, 1 x 1 x 2 cm, 2 x 2 x 2 cm, and 3 x 3 x 3 cm), the Te (30 vs. 150 ms), .and the TR (1.5 vs. 3 sec). The data were examined in the time domain with no preprocessing or corrections applied to the data. Simulated neuronal currents were added to the FID data using the methods described in the Appendix. PLS calibrations of the preprocessed simulated data were used to assess the ability of PLS to quantify the strength of the simulated NC as a function of the various instrument parameters.

2.5. FID Preprocessing Methods

In the absence of a stimulus, each FID can be roughly approximated by an exponentially decaying curve. The visual stimulus is expected to generate a perturbation on the exponential decay curve due to the presence of neuronal current. The nature of this perturbation is unknown. The analysis strategy therefore first removes an exponential decay from each FID. We used log(FID) as the starting point and subtract a linear baseline from each log(FID) signal. In subtracting this linear baseline, the subtracted baseline is pinned at channels 1 and the average of channels 53-57 in the log(FID) data. Data beyond the 53-57 channels becomes dominated by noise, so the baseline to be subtracted is based on these higher signal-to-noise regions of the FID. The corrected data are then trimmed such that only channels 1-55 are analyzed further. This residual log(FID) signal is further corrected for local background effects on a per trial basis. The local background is calculated as the average residual log(FID) for FIDs 1, 3, and 5 in each trial. This average background is then subtracted from FIDs 2, 4, and 6 to correct for small instrument drift effects within a trial. The detection for NC is then based upon statistical tests to determine if the background-corrected 6^{th} log(FID) containing the NC signal is significantly different than the background-corrected 2^{nd} and 4^{th} log(FIDs). PCA was then used to transform these background-corrected spectra to an orthogonal basis. In our subsequent statistical analysis, we considered the scores derived from the first ten PCA eigenvectors. The statistical analysis was based on data sets containing all of the data across all subjects as well as on data sets that had removed trials with large Mahalanobis distances and an insufficient BOLD signal.

2.6. Outlier Detection Methods

We performed two different types of outlier detection in the analyses of these data sets. Outliers are those FIDs that do not conform to the bulk of the FIDs in the experiment. Outlier FIDs may be due motion artifacts, instrument upsets, or other undetermined effects that will cause an FID to be discordant with the others in the experiment. In addition, each trial of 12 FIDs in Experiments 1 and 3 is expected to have the maximum BOLD response present in FIDs 8 and 9. If the BOLD response in the visual cortex is absent after a visual stimulation was presented, then possibly the subject became inattentive or the subject moved sufficiently so that the voxel from which the data were collected was no longer in the center of the visual cortex. In this latter case of an absent BOLD response, the NC would not be expected to be present in the sixth FID of the trial. For either type of outlier, if an outlier FID is present or the BOLD response is absent, the entire trial of 12 FIDs was removed from the analysis.

The first type of outlier was detected using the Mahalanobis distance derived from the set of the first two PCA scores for each FID. The Mahalanobis distance is scaled to the standard deviation for each of the orthogonal PCA score dimensions so that any distance in either dimension that is beyond the expected range of the dimension would be flagged as an outlier. Any significant motion artifact or instrument upset would be expected to be evident in the first two sets of eigenvector scores. Assume that we have a sample of size n from a multivariate normal population with two dimensions with a mean of $\bar{\mu}$ and a covariance of **S**. An F test can be used as the metric to determine if any two-dimensional Mahalanobis distance is an outlier at a confidence level at the 99% level, i.e., what is the probability that a new sample from the same population (y_i) is within the confidence ellipsoid. See Equation 1.

$$f_i = (y_i - \bar{\mu}) S^{-1} (y_i - \bar{\mu})^T \cdot \frac{n(n-2)}{2(n+1)(n-1)} \sim F_{2,n-2} \qquad \text{(Eq. 1)}$$

where $F_{2,n-2}$ is the F-distribution with 2 and n-2 degrees of freedom. The PCA analysis and Mahalanobis distance outlier detection was applied separately to each subject since the various subjects exhibited different levels of variance in their data. In addition, the Mahalanobis distance outlier detection was applied to either the FID data directly or after background correcting the FIDs. Slightly different sets of Mahalanobis distance outliers were identified with the set of original FIDs and the background-corrected FIDs.

The trials where no BOLD response was discernable were also identified for the visual stimulation trials in Experiments 1 and 3. Absence of BOLD response was determined by comparing the response in FIDs 7 and 8 where the maximal BOLD response was expected to be present to the baseline FIDs 1-6 where the BOLD was absent. Since the largest source of variance in the background-corrected data is due to the BOLD response, the first eigenvector will represent primarily the BOLD response. Therefore, we obtain the scores for the first eigenvector for each FID based upon the PCA was conducted on each subject independently using all FIDs in the trials that experienced visual stimulation. The BOLD response was considered to be absent if the mean of the scores for FIDs 8 and 9 was not greater than mean plus the pooled standard deviation of the baseline scores for FIDs 1-6 in each trial. If the BOLD response did not pass this threshold, then the BOLD was considered to be absent and the entire trial was removed from the data set. The BOLD response outliers were only defined for the visual stimulation trials since the BOLD response was much reduced for the trials with the auditory stimulus. The final set of trials without outliers present was obtained from the set of trials which did not contain FIDs flagged as Mahalanobis distance outliers and trials where the BOLD was deemed to be present. Data sets with and without outliers present were analyzed with the various methods.

2.7. Analysis Methods for Detection of Neuronal Current

The experimental MRS data that were obtained on the human subjects were processed, analyzed, and visualized using Matlab code written in house (Matlab version 2010). Various analysis methods were used to search for the NC signal in the data. These analysis methods included principal components analysis (PCA) (Jolliffe, 1986), multivariate curve resolution (MCR) (de Juan and Tauler, 2006 and Haaland *et al.*, 2009), binary logistic regression (e.g.,

Agresti, 2002), analysis of variance (ANOVA) (see e.g., Snedecor and Cochran, 1967), and classification and regression trees (CART) (Breiman *et al.*, 1984). We have previously demonstrated that MCR analyses are ideally suited to discovering small changes in the shapes of spectral features (Haaland *et al.*, 2009). In addition, partial least squares (PLS) (Lindberg *et al.*, 1983 and Haaland and Thomas, 1988) and PCA analyses were further explored using in house software programmed in the Array Basic language (GRAMS AI, Thermo Fisher) that is extremely useful for analyzing, visualizing and plotting spectral data as well as performing PLS classifications in the search of the NC signal. For the sake of brevity, we present in detail only those analysis methods whose results will be discussed in more detail in the Results and Discussion Section.

Binary logistic regression was used in two ways in this study. First (Experiments 1 and 3), it was used as a screening tool to help evaluate the ability of the various PCA-determined dimensions to help discriminate between FID-6 (which contains the NC signal) and FIDs-2,4 (which do not contain the NC signal). Binary logistic regression was also used to try to discriminate between FID's arising from a visual stimulus versus an auditory stimulus (Experiments 2 and 3) using the various PCA-determined dimensions. In binary logistic regression, the probability associated with a binary outcome is modeled as a function of explanatory variables using the logit function. That is, $\text{Log}(P/(1-P) = f(\text{explanatory variables})$, where P is the probability of a particular binary outcome. In the first use of binary logistic regression, the binary outcome is either Y=0 (when FID-2 or FID-4) or Y=1(when FID-6). In the second use of binary logistic regression, the binary outcome is either Y=0 (auditory stimulus) or Y=1(visual stimulus). In both cases, the explanatory/predictor variables were the 10 PCA-determined dimensions. The actual logistic regression analyses were performed in MINITAB.

Analysis of variance (ANOVA) is a general statistical method in which the observed variance in a particular response variable is partitioned and assigned to different sources. With modest assumptions, ANOVA can help determine whether or not a particular factor has a significant influence on the response of interest. Here, we use ANOVA to determine if the FID (2 versus 4 versus 6) within a trial (involving a visual stimulus) has a significant influence on certain PCA-determined dimensions. An underlying assumption is that the only difference between (FID's 2 and 4) and FID 6 is that FID-6 contains the NC signal. So if we find that FID-6 produces a distinct effect (statistically significant) on a particular PCA dimension, then that is evidence for the detection of the NC signal. We would also conclude that the NC signal is related to the eigenvector (PCA loading vector) that gives rise to that dimension.

3. RESULTS AND DISCUSSION

3.1. Analyses of the Agar Phantom Data

PCA analysis of the agar phantom real data in the spectral domain was performed for all the instrument conditions studied. The PCA score plots as a function of time showed that instrumental drift was often present in the data, but they also indicated a consistent discontinuity exactly in the middle of the sets of 120 FIDs in the agar phantom data when instrument drift was present. Further investigation of this phenomenon identified an error in the reconstruction of the data from the Seimans MRS instrument. By correctly reordering the data, the discontinuity in the data was eliminated (see Figure 4). Without the data from this agar phantom study, the data would not have been properly assembled, and it would have been impossible to detect NC in any human study. The results of the analysis indicated that noise variance in the FID was constant across all time points in the FID. In addition, the water spectral signal was directly proportional to the volume of the pixel and FIDs with a Te = 30 ms gave an order of magnitude increase in signal relative to FIDs with a Te of 150 ms. Changes in TR from 1.5 s to 3 s resulted in ~10% change in FID intensity whereas the location of the voxel in the center or at the edge of the agar phantom had only slight differences that were possibly masked by instrument drift. PLS analysis of the Te = 30 vs 150 ms NC simulated phantom data confirmed the greater detection ability of NC when Te = 30 ms relative to Te = 150 ms. In comparison, the human phantom data demonstrate that the human subject data are significantly more complex than the agar phantom data. This greater noise and complexity is demonstrated in the scree plot in Figure 5 which compares log(eigenvalue) as a function of factor number derived from an eigenvector (PCA) decomposition of the human phantom data relative to that of the agar phantom when Te = 30 ms.

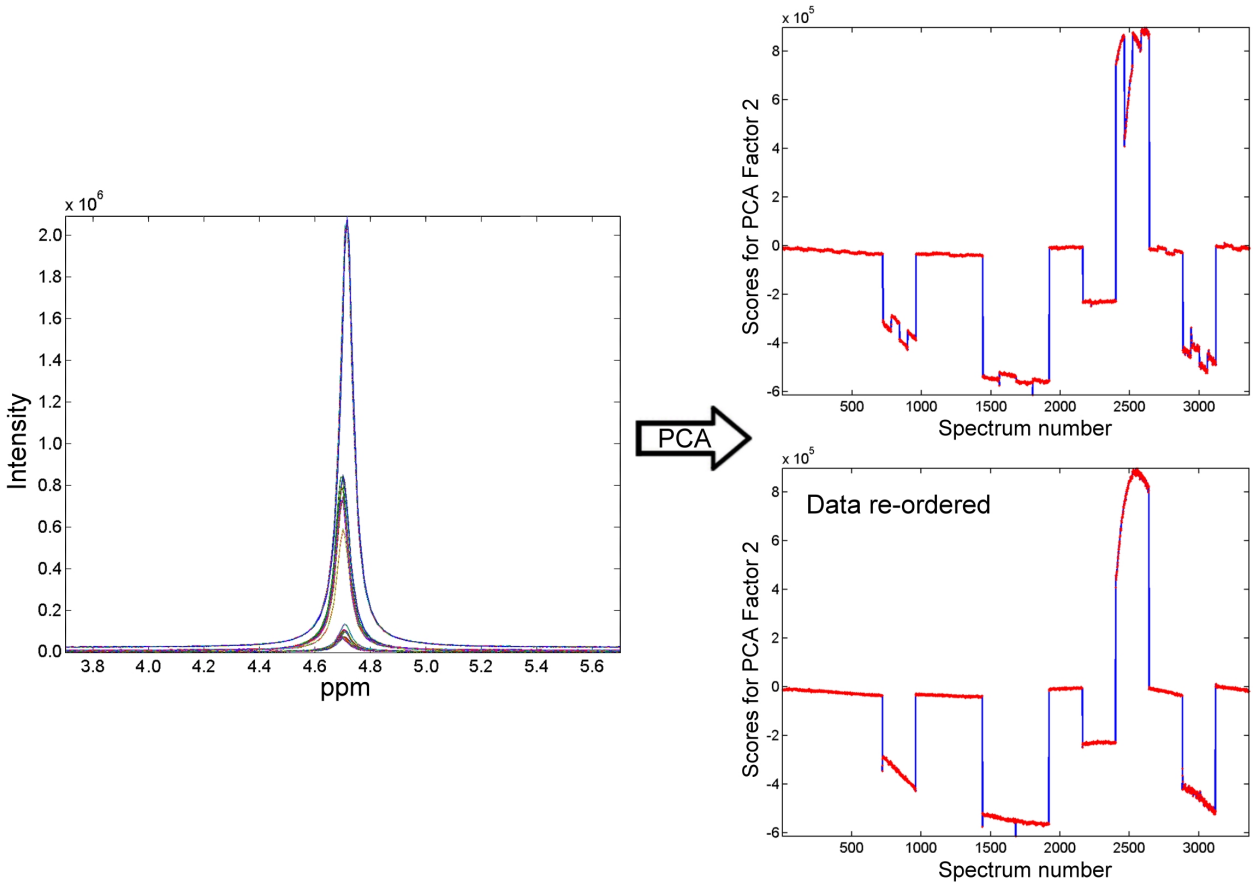

Figure 4. PCA analysis of the agar phantom real data (spectral domain) showing the scores of factor 2 with incorrect ordering of FID data (top plot) and scores reordered correctly (bottom plot).

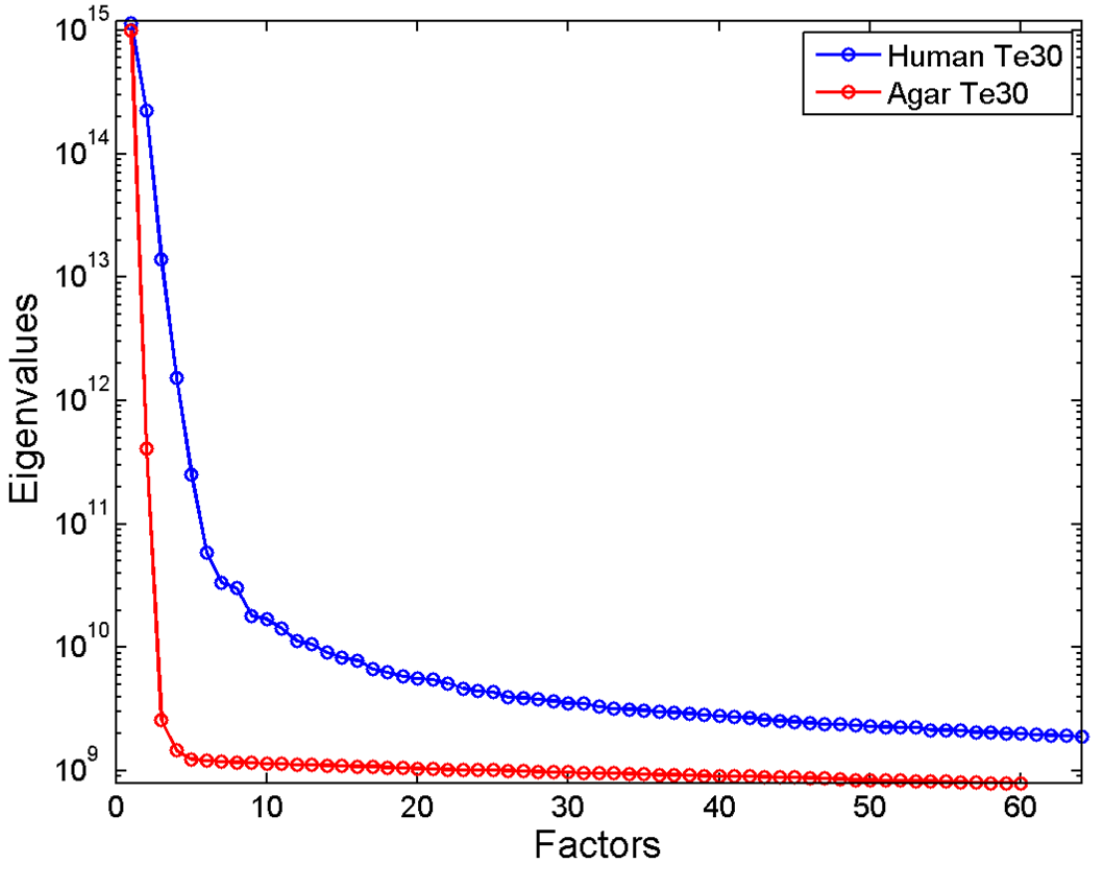

Figure 5. Logarithmic transformation of the eigenvalues derived from a PCA decomposition of human phantom data relative to that of the agar phantom.

3.2. Human Phantom Study

Our simulated NC human phantom data were used to investigate the ability of data preprocessing to minimize the effects of instrumental drift and to improve detection of the simulated NCs. We found that instrumental drift that was readily apparent in the real and imaginary data could be greatly minimized with optimized preprocessing of the raw data. The optimal preprocessing method was identified as that preprocessing method that minimized the prediction error for detecting the presence of the FIDs with NC present during cross-validated PLS classifications. FID 6 with NC present was assigned a class of 1 while all other FIDs with NC absent were assigned a class of 0 in these PLS classification models. The optimal preprocessing that yielded the best detection of NC included the steps of phase correction of the data to that of the first FID collected in a trial, correcting shifts in the MRS water peak in the real spectra after 16 times zero padding of the FIDs, Fourier transforming the zero padded FIDs with exponential apodization followed by shifting the water spectral peak to match the location of the water spectral peak for the first collected spectrum of a trial. In addition, we maximized the signal-to-noise ratio by truncating the FIDs from 1024 to 128 data points before performing the

final FFT. These same simulated NC investigations demonstrated that the magnitude data were far less sensitive to time-dependent instrument drift relative to either the real or the imaginary portions of the FIDs. There were no statistically significant differences in the ability of PLS classification to detect the presence or absence of the NC independent of using optimally preprocessed real FID data or magnitude FID data. The nonparametric Wilcoxon signed rank test (Lehmann, 1975) was used to determine that the prediction abilities were statistically indistinguishable for either the magnitude or optimally preprocessed real FID data. In addition, we found no difference in detection ability of the simulated human phantom magnitude data whether we worked with the data in the original FID time domain or after the data were Fourier transformed to the spectral domain. Therefore, in the final analysis of the experimental NC human data, magnitude data were used in the analyses without any preprocessing other than phase correction. Although the periodic respiration was clearly observed in both the original real and imaginary data, the use of either magnitude data or optimally preprocessed real or imaginary data eliminated the interfering effects of respiration on the data. Evidence of the heart beat was not clearly discerned in the FID data probably because the effects on the FID are smaller than those of respiration and the fact that the heart beat rate was faster than the rate of collection of the FIDs. In any case, like the respiration, residual perturbations of the FIDs by the heart beat would be minimized when analyzing optimally preprocessed MR spectra or magnitude FID data.

3.3. NC Experiment 1 (10 subjects)

3.3.1. Analysis of the BOLD Signal

We analyzed the magnitude FID data for each subject separately to confirm our hypothesis that the BOLD signal was not present in the first 5 FIDs of repeated sets of trials consisting of 12 FIDs with stimulation occurring at FID 6 in each trial. We examined all the data that was background-corrected within each trial and performed analyses for each subject separately. Since the BOLD is the largest source of variation in the FIDs, its influence on the background-corrected FIDs is captured in the mean background-corrected FID signal for each subject. Combined all-subject box plots of these background-corrected FID means for the third experiment are shown in Figure 6. The box plot for each FID position gives the range of the data, the 25^{th} and 75^{th} percentiles of the samples as the tops and bottoms of each box. The red line in the middle of the box is the median, and the width of the notch represents two standard deviations of the data in each box. A visual examination of the box plot of scores demonstrates that the BOLD signal in these plots is first apparent at FID 7, peaks at FID 8, and is again at baseline for FIDs 12 and FIDs 1 through 5 since there are no statistically significant differences between the means of FIDs 1-5 and 12 at the 0.05 level. Thus, we were able to use FIDs 1, 3, and 5 for defining our baseline FID in our various search approaches for detecting the NC in the FID data.

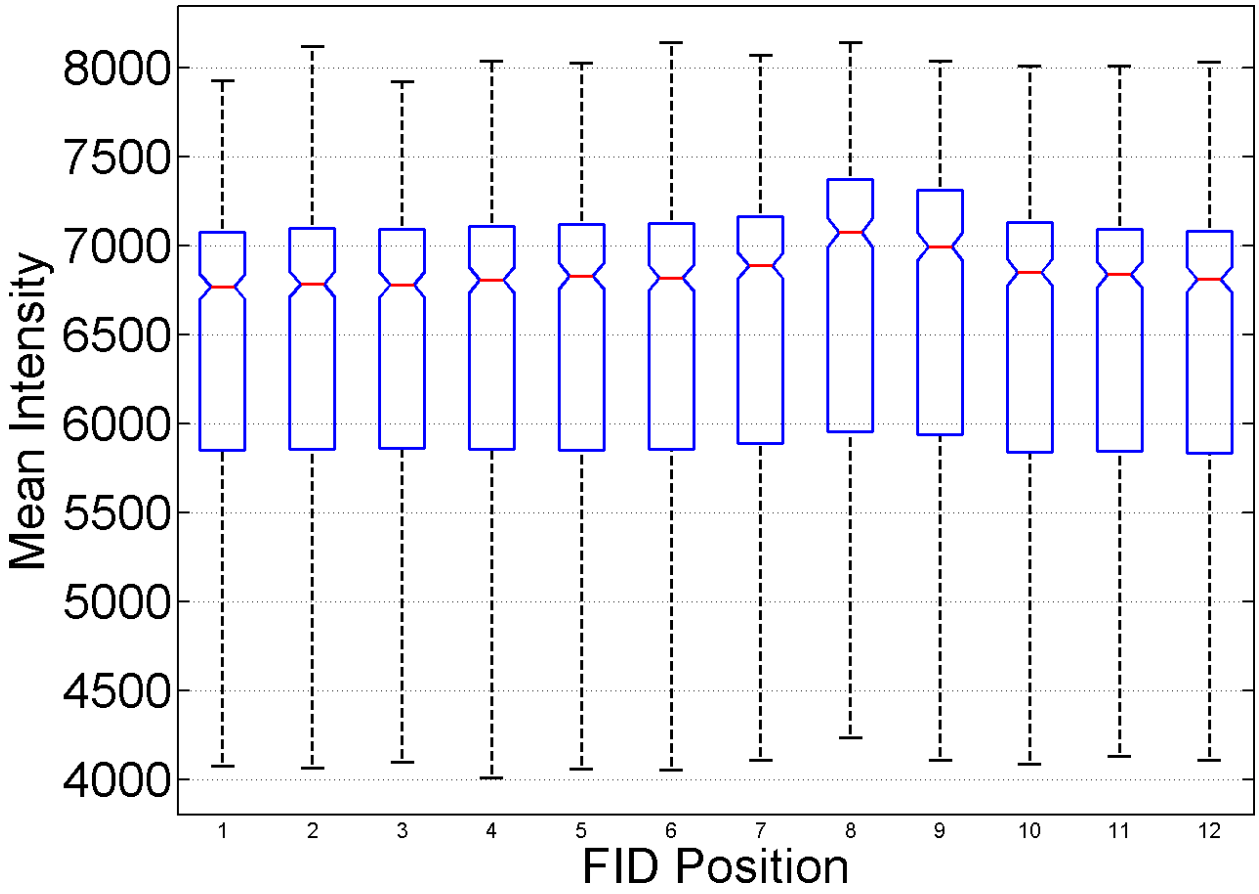

Figure 6. Combined mean intensities of each FID across all subjects shown as a function of FID position within experiment 1.

3.3.2. Analysis of Experiment 1

A variety of analysis methods were applied to the magnitude FID data for our 10 subject data with and without visual stimulation present while monitoring a single voxel in the visual cortex. In our search for evidence of NC in the 6th FID of each trial for the entire data set, several different analysis methods indicated statistically significant differences in the signal present in this FID where the NC should be present relative to the background FIDs. Multivariate curve resolution (MCR) analysis, logistic regression, and ANOVA analysis all suggested the presence of a statistically significant difference between background-corrected FID 6 relative to background-corrected FIDs 2 and 4. PLS and CART classification analyses were also applied to the FID data, but no classification was possible with either of these classification methods. For the sake of conciseness and statistical rigor, only the details of the logistic regression and ANOVA results will be discussed in detail here.

The logistic regression and ANOVA analyses were performed on the background-corrected log(FID) data after removal of the linear portion of the log(FID) data as described in the Methods Section. The goal of the both the logistic regression and ANOVA applied to the data was to find if there were statistically significant differences between background-corrected FID 6 where the

NC should reside and the background-corrected FIDs 2 or 4 where the NC should be absent. Logistic regression and ANOVA were both used to analyze the full data set as well as the data set with Mahalanobis distance and BOLD outlier FID trials removed. The analysis was limited to the PCA scores for the first 10 orthogonal loading vectors (eigenvectors) derived from the background-corrected FID data. We restricted our evaluation to the first 10 PCA scores since the scree plot (Cattell, 1966.) of the log of the eigenvalues versus principal component number indicates that the signals decay into the noise before this limit of 10 scores is reached. Tables 1 and 2 show the results of the logistic regression analysis for the full data set and the outlier deleted data set, respectively. In both these cases, the p-values associated with the scores of eigenvector 2 were significant (p-values < 0.05) for discriminating between FID 6 relative to FIDs 2 and 4. Removing the outlier trials slightly increased the statistical significance of eigenvector 2 in the logistic regression (P = 0.021 vs. P =0.014 without outliers). None of the other 9 PCA-dimensions (scores) were found to exhibit statistically significant differences between FID 6 and the baseline FIDs 2 and 4. See Figure 7 for a plot of the second eigenvector for the case when outliers were removed. The shape of this second eigenvector is characteristic of a shift in the rate of decay of the FID for FID 6 versus FIDs 2 and 4. Our MCR analyses of the data set with outliers removed also indicated a shift in the decay rate of the FID for FID 6 relative to that of FIDs 2 and 4. The presence of NC is expected to change the rate of decay of the FID, so these observations are consistent with the presence of NCs.

Table 1. Summary of Logistic Regression Analysis (Experiment 1, All Trials)[a]

Predictor	Coefficient[b]	SE Coefficient[c]	Z[d]	P-value[e]
Constant	-0.697	0.0458	15.21	0.000
Score 1	3.91	2.42	1.62	0.106
Score 2	-14.2	6.17	-2.31	**0.021**
Score 3	-6.61	9.13	-0.72	0.469
Score 4	12.2	11.1	1.09	0.274
Score 5	1.90	11.7	0.16	0.871
Score 6	-7.85	13.0	-0.61	0.545
Score 7	12.8	13.5	0.95	0.342
Score 8	-0.748	14.6	-0.05	0.959
Score 9	0.845	15.2	0.05	0.959
Score 10	-1.30	15.8	-0.08	0.935

a. 720 observations with Y=1 and 1440 observations with Y=0.
b. Coefficient for Logistic Regression Predictor
c. Standard Error of the Coefficient for Predictor
d. Z=Coefficient/(SE Coefficient)
e. P-value = Probability of observing such a large effect (absolute value of coefficient) by chance (P-value < 0.05 highlighted in red/bold)

Table 2. Summary of Logistic Regression Analysis (Experiment 1, Trials Without Outliers)[a]

Predictor	Coefficient[b]	SE Coefficient[c]	Z[d]	P-value[e]
Constant	-0.697	0.0499	-13.95	0.000
Score 1	4.01	3.06	1.31	0.190
Score 2	-17.8	7.24	-2.46	**0.014**
Score 3	-0.366	11.0	-0.03	0.974
Score 4	8.37	12.8	0.65	0.515
Score 5	-5.35	13.8	-0.39	0.697
Score 6	7.28	15.2	0.48	0.632
Score 7	-7.07	16.4	-0.43	0.667
Score 8	11.4	17.5	0.65	0.516
Score 9	9.95	18.1	0.55	0.582
Score 10	-1.48	18.5	-0.08	0.936

a. 606 observations with Y=1 and 1212 observations with Y=0.
b. Coefficient for Logistic Regression Predictor
c. Standard Error of the Coefficient for Predictor
d. Z=Coefficient/(SE Coefficient)
e. P-value = Probability of observing such a large effect (absolute value of coefficient) by chance (P-value < 0.05 highlighted in red/bold)

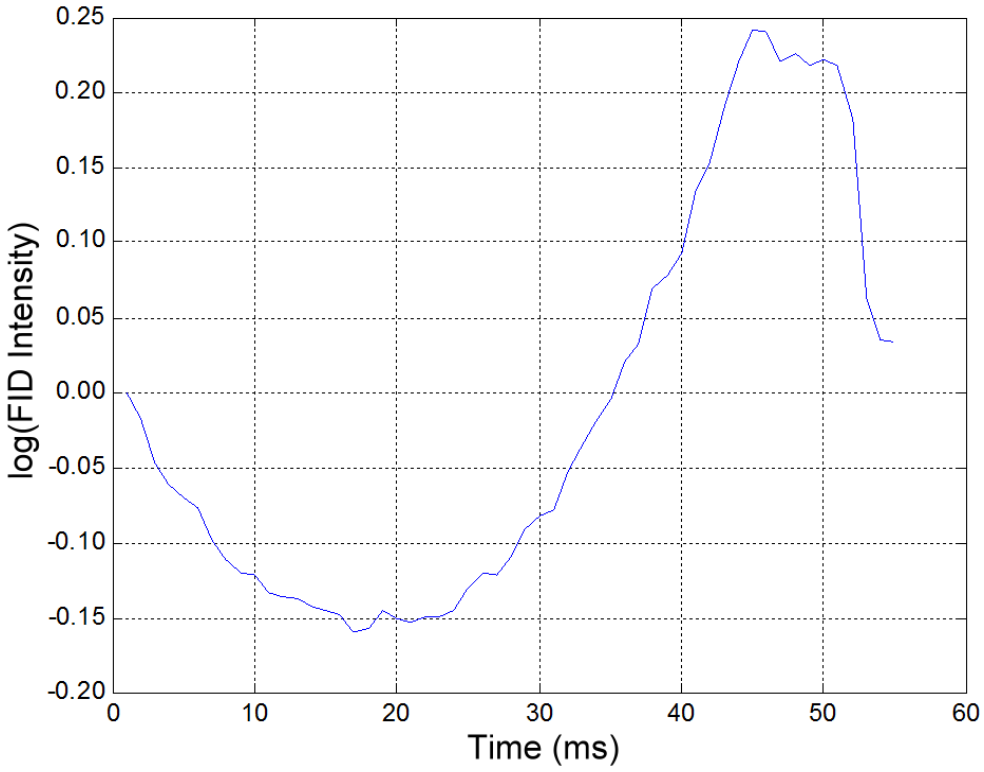

Figure 7. Statistically Significant Eigenvector 2 for Experiment 1

We achieved a similar result by using ANOVA to analyze the effect of FID (2 versus 4 versus 6) on the scores for PCA factor 2. For this analysis, we also accounted for small residual effects specific to a trial not already removed by the background correction. The results of the ANOVA analyses are shown in Tables 3 and 4 for the full data set and for the data set with outliers removed, respectively. The specific contrast among FIDs that is significant is the contrast between FID 6 and FIDs 2 and 4 (see Figure 8). It is important to point out that the apparent "FID effect" was not broadly observed across all subjects.

Table 3. Analysis of Variance (Experiment 1, Full Data Set)[a]

Source	**DF[b]**	**SS[c]**	**Adj SS[d]**	**Adj MS[e]**	**F[f]**	**P-value[g]**
SRT[h]	719	0.0427	0.0427	0.000059	1.12	0.043
FID	2	0.00033	0.00033	0.00016	3.07	**0.047**
Error	1438	0.0768	0.0766	0.000053		
Total	2159	0.120				

a. Analysis of variance to assess effect of FID (2 versus 4 versus 6) on Score 2 adjusted by trial (SRT)
b. Degrees of freedom
c. Sum of squares
d. Adjusted sum of squares
e. Adjusted Mean Square = d / b
f. F-value = e(Source) / e(Error)
g. P-value = Probability of observing such a large effect (due to Source term) by chance (P-value < 0.05 highlighted in red/bold)
h. SRT is the common effect of Subject/Run/Trial across back-ground-corrected FID's 2, 4, and 6

Table 4. Analysis of Variance (Experiment 1, Data Set with Outliers Removed)[a]

Source	DF[b]	SS[c]	Adj SS[d]	Adj MS[e]	F[f]	P-value[g]
SRT[h]	605	0.0305	0.0305	0.000050	1.09	0.115
FID	2	0.00030	0.00030	0.00015	3.29	**0.038**
Error	1210	0.0561	0.0561	0.000046		
Total	1817	0.0869				

a. Analysis of variance to assess effect of FID (2 versus 4 versus 6) on Score 2 adjusted by trial (SRT)
b. Degrees of freedom
c. Sum of squares
d. Adjusted sum of squares
e. Adjusted Mean Square = d / b
f. F-value = e(Source) / e(Error)
g. P-value = Probability of observing such a large effect (due to Source term) by chance (P-value < 0.05 highlighted in red/bold)
h. SRT is the common effect of Subject/Run/Trial across back-ground-corrected FID's 2, 4, and 6

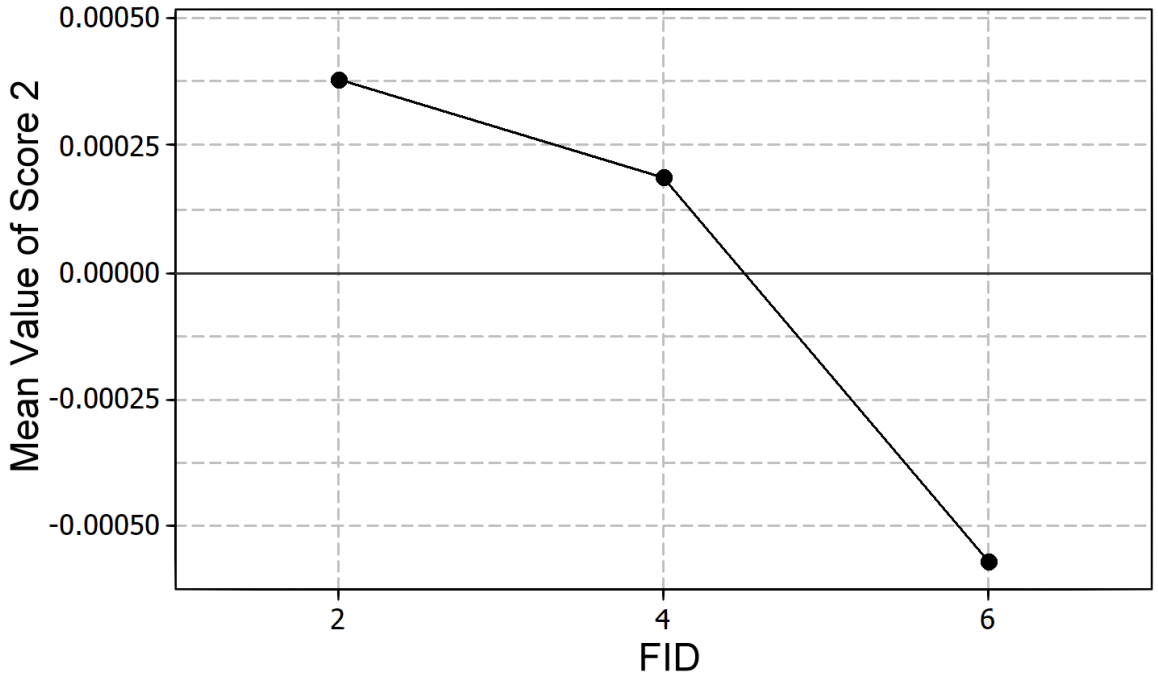

Figure 8. Main Effects Plot for the scores of eigenvector 2 (case with outliers removed)

However, even with all these tests demonstrating statistical significance, they are not conclusive of the presence of NCs in the FIDs where they are expected. It is possible that these significant differences in variance between background-corrected FID 6 vs. FIDs 2 and 4 are due

to some other phenomenon such as a startle response to the stimulus. In order to further explore these initially positive results, we designed two additional experiments to both replicate these results and to more fully understand the differences observed.

3.4. NC Experiment 2 (10 subjects)

This experiment was designed to both determine if the NC could be observed in the presence of the BOLD response as well as to confirm that any statistically significant differences observed in the FIDs with NC present could be confirmed to be due to the NC itself and not due to some other spurious effect. Also, being able to detect the NC in the presence of the BOLD response would be required in any practical ncMRI imaging experiment. As described in the Methods Section, these experiments consisted of trials of 3 FIDs obtained with a TR of 500 ms and with the stimulus presented in the first FID of each trial. Thus, the BOLD signal would be present in all trials as we attempt to mitigate its detrimental effects through saturation. Both visual and auditory stimuli were presented in separate runs during these studies so that spurious effects such as startle could be eliminated by comparisons of the responses between the visual and auditory stimulation while monitoring the visual cortex as in Experiment 1. The rapid presentation of the stimuli would also be expected to reduce any startle response in these experiments. In addition, both the visual and auditory stimuli were each presented with two different delay times relative to the start of the FID so that the location of the NC in the FID would vary with the two delay times. Thus, any observed shift in the FID decay curve would need to be consistent with the timing changes in the stimuli in order for NC detection to be confirmed.

The preprocessing of the magnitude FID data was similar to that of Experiments 1 and 3, except that the NC resided in FID 1 and the mean of FIDs 1 and 2 was used to perform the background correction. Again MCR, logistic regression, ANOVA, and PLS were applied to the full data set and to the reduced data with outliers removed. Unfortunately, in the analyses of these experiments, none of the tests or analyses demonstrated any statistically significant differences between the background-corrected FIDs containing the NC and those without NC present. Since we had both visual and auditory stimuli present in Experiment 2, we could also compare the background-corrected FIDs with visual stimulus to those containing the auditory stimulus. Again, none of the above tests yielded any statistically significant differences between FIDs with visual vs. auditory stimulation. Multiple MCR analyses also failed to find the differences in FID decay rates that were found in Experiment 1.

It is possible that the slightly oscillatory behavior of the BOLD signal in this experiment dominated the NC effects in the FIDs and rendered its detection difficult. It is also possible that the shorter TR= 0.50 s vs. TR= 3 sec, which leads to a smaller FID signal, reduced the signal-to-noise ratio of the NC signal in the FID data. It had been hoped that the larger number of trials in this study relative to Experiment 1 would have served to counter this lower FID signal. In any case, no differences in the FIDs when NC was expected to be present could be found when compared to FIDs where NC was expected to be absent.

3.5. NC Experiment 3 (11 subjects)

In order to further attempt to replicate the positive results of Experiment 1 and to rule out startle response as a source for the significant differences found between the NC containing FID and the baseline FIDs, we designed a third experiment. This third NC experiment, which is carefully described in the Methods Section, was a close replicate of first experiment and like the Experiment 1; it had BOLD response absent in the first 6 FIDs. Experiment 3 also had several modifications relative to Experiment 1. In this third experiment, half of the stimulation trials used visual stimulation and the other half used auditory stimulation. We also added one additional subject to the study for a total of 11 subjects. Three of the subjects were the same for both Experiments 1 and 3. Finally, we replicated all our MRS experimental parameters from Experiment 1 in Experiment 3. Unfortunately, the performance of the phototransistor measuring the onset of the visual stimulus was erratic in this experiment. Its data would seem to indicate that the visual stimulus in Experiment 3 may have occurred at a time centered at approximately 15 ms earlier in the FID than in Experiment 1. It is not known if the poor performance of the phototransistor was not able to reliably indicate the onset of the stimulus and the visual stimulation was actually at the same location in the FID as occurred in Experiment 1 or if the visual stimulation actually occurred at this earlier time in the FID. Based upon PLS analyses of our human phantom simulations, a stimulus placed at the earlier location in the FID would have a slightly lower delectability than at the 35 ms location of the NC in Experiment 1. Nevertheless, we subjected the background-corrected data to all the same analysis procedures as before, but unlike Experiment 1, comparisons between the responses to the two different stimuli at FID 6 could be also made for both the visual and auditory stimuli in this third experiment.

Contrary to the results of the first experiment, neither the logistic regression nor the ANOVA analysis of Experiment 3 demonstrated any statistically significant differences in the eigenvector scores between background-corrected FID 6 and FIDs 2 and 4 for any of the first set of 10 eigenvectors. See Tables 5 and 6 for logistic regression results for the full data set and the data set with outliers removed, respectively. Also, Tables 7 and 8 show the ANOVA results for these same data. As in Experiment 1, the PLS classification method did not exhibit any statistically significant differences between the background-corrected sixth FIDs and the background-corrected FIDs 2 and 4. In addition, no statistically significant differences were found with the any of these three methods when the background-corrected auditory and visual stimulation FIDs 6 were compared. Extensive MCR analyses were also performed on these data, but again no differences were found either between background-corrected FIDs 2 and 4 and FID 6 containing the NC. Finally, MCR did not find any differences between background-corrected FID 6 in the visual vs. auditory trials.

Table 5. Summary of Logistic Regression Analysis (Experiment 3, All Trials)[a]

Predictor	Coefficient[b]	SE Coefficient[c]	Z[d]	P-value[e]
Constant	-0.697	0.0588	-11.87	0.000
Score 1	3.94	3.39	1.16	0.245
Score 2	-12.1	9.56	-1.26	0.206
Score 3	-3.45	14.5	-0.24	0.812
Score 4	-2.95	15.9	-0.19	0.853
Score 5	11.3	17.3	0.66	0.512
Score 6	-20.6	18.1	-1.14	0.254
Score 7	0.835	19.2	0.04	0.965
Score 8	4.49	20.9	0.22	0.829
Score 9	1.82	21.3	0.09	0.932
Score 10	-0.683	22.3	-0.03	0.976

a. 440 observations with Y=1 and 880 observations with Y=0.
b. Coefficient for Logistic Regression Predictor
c. Standard Error of the Coefficient for Predictor
d. Z=Coefficient/(SE Coefficient)
e. P-value = Probability of observing such a large effect (absolute value of coefficient) by chance (P-value < 0.05 highlighted in red/bold)

Table 6. Summary of Logistic Regression Analysis (Trials Without Outliers)[a]

Predictor	Coefficient[b]	SE Coefficient[c]	Z[d]	P-value[e]
Constant	-0.701	0.0703	-9.98	0.000
Score 1	-6.20	4.00	-1.55	0.121
Score 2	0.793	11.6	0.07	0.945
Score 3	-13.0	18.0	-0.72	0.471
Score 4	6.70	18.6	0.36	0.719
Score 5	0.813	21.9	0.04	0.970
Score 6	20.0	21.9	0.92	0.360
Score 7	-5.94	22.7	-0.26	0.794
Score 8	2.95	24.5	0.12	0.904
Score 9	-29.6	26.3	-1.12	0.261
Score 10	-6.13	26.6	-0.23	0.818

a. 309 observations with Y=1 and 618 observations with Y=0.
b. Coefficient for Logistic Regression Predictor
c. Standard Error of the Coefficient for Predictor
d. Z=Coefficient/(SE Coefficient)
e. P-value = Probability of observing such a large effect (absolute value of coefficient) by chance (P-value < 0.05 highlighted in red/bold)

Table 7. Analysis of Variance (Experiment 3, Full Data Set)[a]

Source	DF[b]	SS[c]	Adj SS[d]	Adj MS[e]	F[f]	P-value[g]
SRT[h]	439	0.0224	0.0224	0.000051	1.66	0.000
FID	2	0.000067	0.000067	0.000034	1.09	**0.336**
Error	878	0.0270	0.0270	0.000031		
Total	1319	0.0495				

a. Analysis of variance to assess effect of FID (2 versus 4 versus 6) on Score 2 adjusted by trial (SRT)
b. Degrees of freedom
c. Sum of squares
d. Adjusted sum of squares
e. Adjusted Mean Square = d / b
f. F-value = e(Source) / e(Error)
g. P-value = Probability of observing such a large effect (due to Source term) by chance
h. SRT is the common effect of Subject/Run/Trial across back-ground-corrected FID's 2, 4, and 6

Table 8. Analysis of Variance (Experiment 3, Data Set with Outliers Removed)[a]

Source	DF[b]	SS[c]	Adj SS[d]	Adj MS[e]	F[f]	P-value[g]
SRT[h]	308	0.0150	0.0150	0.0000487	1.57	0.000
FID	2	0.0000043	0.0000043	0.0000022	0.07	**0.932**
Error	616	0.0191	0.0191	0.0000310		
Total	926	0.0341				

a. Analysis of variance to assess effect of FID (2 versus 4 versus 6) on Score 2 adjusted by trial (SRT)
b. Degrees of freedom
c. Sum of squares
d. Adjusted sum of squares
e. Adjusted Mean Square = d / b
f. F-value = e(Source) / e(Error)
g. P-value = Probability of observing such a large effect (due to Source term) by chance
h. SRT is the common effect of Subject/Run/Trial across back-ground-corrected FID's 2, 4, and 6

4. CONCLUSIONS

The task of searching for the NC signal in the MR data was embarked upon as a high risk, high payoff project. Numerous studies in the past have failed to find evidence of the NC when using magnetic resonance imaging applied to normal human subject with various stimuli presented (see the Introduction for a review of this literature). We chose to take a fundamentally different approach than has been used in the past. Instead of using MRI approaches, we chose to examine the subtle changes in the FIDs obtained in MRS of a fixed voxel in the subjects caused by the presence of stimulus induced neuronal currents. Our previous experience with statistical approaches and MCR methods applied to various spectral data gave us the tools to detect and identify extremely small changes in the data due to perturbations. Our initial human subject experiments examining a single voxel in the visual cortex during visual stimulation in the absence of BOLD response yielded statistically significant differences between the FIDs with the NC present and those FIDs where it was absent. The changes in the shape of the FIDs were consistent with changes expected from NC, but other causes for the differences, such as a startle response, could not be ruled out in these data. Two subsequent experiments with BOLD present and BOLD absent used auditory stimulation as a control to eliminate startle as the cause of the mild significant differences in the first experiment. Unfortunately, neither of studies was able to replicate our initial positive result.

Experiment 3attempted to replicate Experiment 1 but added an auditory stimulus as a control. It is not clear why we did not replicate the statistically significant differences in Experiment 3 that we found in the first experiment. If the positive results from the first experiment were due to a startle response, we might have expected to see it in this third experiment also. However, we did not observe any significant differences in response either between the background-corrected FID 6 vs. FID 2 or 4 or between FID 6 with the visual vs. auditory stimuli present. It is possible that the lower numbers of visual stimulus trials in the second experiment led to this non-significant result or that the significant result of the first experiment was due to chance. It is also possible that the location of the NC relative to the start of the FID, which may have been approximately15 ms earlier than in Experiment 1, reduced our ability to detect the NC in Experiment 3 relative to Experiment 1. Without a positive finding in the Experiment 3, we can only speculate as to the differences between the outcomes of the two experiments. However, even if the result from the first experiment were evidence of the presence of NC in the FID, it is clear that its effect is so small on the FID, that a true NC imaging experiment would not be possible with the current instrumentation and experimental protocol that we used here.

4. REFERENCES

Agresti, A., 2002. Categorical Data Analysis, Wiley-Interscience, New York, NY.

Bandettini, P. A., Jesmanowicz, A., van Kylen, J., Birn, R.M., Hyde, J.S., 1998. Functional MRI of brain activation induced by scanner acoustic noise. Magn. Reson. Med. 39, 410-416.

Bandettini, P.A., Petridou, N., Bodurka, J., 2005. Direct detection of neuronal activity with fMRI: Fantasy, possibility, or reality? Appl. Magn. Reson. 29, 65-88.

Blagoev, K.B., Mihaila, B., Travis, B.J., Alexandrov, L.B., Bishop, A.R., Ranken, D., Posse, S., Gasparovic, C., Mayer, A., Aine, C.J., Ulbert, I., Morita, M., Muller, W., Connor, J., Halgren, E., 2007. Modelling the magnetic signature of neuronal tissue. Neuroimage 37, 137-148.

Bodurka, J., Jesmanowicz, A., Hyde, J.S., Xu, H., Estkowski, L., Li, S.J., 1999. Current-induced magnetic resonance phase imaging. J. Magn. Reson. 137, 265-271.

Breiman, L., Friedman, J. H., Olshen, R. A., Stone, C. J., 1984. Classification and Regression Trees. Wadsworth & Brooks/Cole Advanced Books & Software, Monterey, CA.

Cassara, A.M., Hagberg, G.E., Bianciardi, M., Migliore, M., Maraviglia, B., 2008. Realistic simulations of neuronal activity: a contribution to the debate on direct detection of neuronal currents by MRI. Neuroimage 39, 87-106.

Cattell, R.B., 1966. The scree test for the number of factors. Multiv. Behav. Res., 1, 245–276.

Chu, R., de Zwart, J.A., van Gelderen, P., Fukunaga, M., Kellman, P., Holroyd, T., Duyn, J.H., 2004. Hunting for neuronal currents: absence of rapid MRI signal changes during visual-evoked response. Neuroimage 23, 1059-1067.

Cohen, M., 1997. Parametric analysis of FMRI data using linear systems methods. NeuroImage 6, 93-103.

Cox, R.W., 1996. AFNI: software for analysis and visualization of functional magnetic resonance neuroimages. Comput. Biomed. Res. 29, 162-173.

de Juan, A., Tauler, R., 2006. Multivariate curve resolution (MCR) from 2000: Progress in concepts and applications. Crit. Rev. Anal. Chem. 36, 163-176.

Feng, Z., Caprihan, A., Blagoev, K.B., Calhoun, V.D., 2009. Biophysical modeling of phase changes in BOLD fMRI. Neuroimage 47, 540-548.

Haaland, D.M., Thomas, E.V., 1988. Partial least squares methods for spectral analyses 1: relation to other multivariate calibration methods and the extraction of qualitative information. Anal. Chem. 60, 1193-1202.

Haaland, D.M., Howland J.D.T., van Benthem, M.H., Sinclair, M.B., Melgaard, D.K., Stork, C.L., Pedroso, M.C., Liu, P., Brasier, A.R., Andrews, N.L., Lidke, D.S., 2009. Hyperspectral confocal fluorescence imaging: exploring alternative multivariate curve resolution approaches. Appl. Spectrosc. 63, 271-279.

Hagberg, G.E., Bianciardi, M., Brainovich, V., Cassara, A.M., Maraviglia, B., 2008. The effect of physiological noise in phase functional magnetic resonance imaging: from blood oxygen level-dependent effects to direct detection of neuronal currents. Magn. Reson. Imaging 26, 1026-1040.

Hagberg, G.E., Bianciardi, M., Maraviglia, B., 2006. Challenges for detection of neuronal currents by MRI. Magn. Reson. Imaging 24, 483-493.

Hamalainen, M., Hari, R., Ilmoniemi, R., Knuutila, J., Lounasmaa, O., 1993. Magnetoencephalography–theory, instrumentation, and applications to noninvasive studies of the working human brain. Rev. Mod. Phys. 65, 413-497.

Heller, L., Barrowes, B.E., George, J.S., 2009. Modeling direct effects of neural current on MRI. Hum. Brain Mapp. 30, 1-12.

Hennig, J., Ernst, T., Speck, O., Deuschl, G., Feifel, E., 1994. Detection of brain activation using oxygenation sensitive functional spectroscopy. Magn. Reson. Med. 31, 85-90.

Jolliffe, I.T., 1986. Principal Component Analysis. Springer-Verlag, New York, NY.

Kamei, H., Iramina, K., Yoshikawa, K., Ueno, S., 1999. Neuronal current distribution imaging using magnetic resonance. IEEE Trans. Magnetics 35, 4109-4111.

Kim, D.S., Ronen, I., Olman, C., Kim, S.G., Ugurbil, K., Toth, L.J., 2004. Spatial relationship between neuronal activity and BOLD functional MRI. Neuroimage 21, 876-885.

Konn, D., Gowland, P., Bowtell, R., 2003. MRI detection of weak magnetic fields due to an extended current dipole in a conducting sphere: a model for direct detection of neuronal currents in the brain. Magn. Reson. Med. 50, 40-49.

Kraus, R.H., Jr., Volegov, P., Matlachov, A., Espy, M., 2008. Toward direct neural current imaging by resonant mechanisms at ultra-low field. Neuroimage 39, 310-317.

Lindberg, W., Persson, J.-A., Wold, S., 1983. Partial least-squares method for spectrofluorimetric analysis of mixtures of humic-acid and ligninsulfonate. Anal. Chem. 55, 643-648.

Liston, A.D., Salek-Haddadi, A., Kiebel, S.J., Hamandi, K., Turner, R., Lemieux, L., 2004. The MR detection of neuronal depolarization during 3-Hz spike-and-wave complexes in generalized epilepsy. Magn. Reson. Imaging 22, 1441-1444.

Logothetis, N.K., 2002. The neural basis of the blood-oxygen-level-dependent functional magnetic resonance imaging signal. Philos. Trans. R Soc. Lond. B Biol. Sci. 357, 1003-1037.

Logothetis, N.K., 2008. What we can do and what we cannot do with fMRI. Nature 453, 869-878.

Logothetis, N.K., Pauls, J., Augath, M., Trinath, T., Oeltermann, A., 2001. Neurophysiological investigation of the basis of the fMRI signal. Nature 412, 150-157.

Luo, Q., Jiang, X., Chen, B., Zhu, Y., Gao, J.H., 2011a. Modeling neuronal current MRI signal with human neuron. Magn. Reson. Med. 65, 1680-1689.

Luo, Q., Jiang, X., Gao, J.H., 2011b. Detection of neuronal current MRI in human without BOLD contamination. Magn. Reson. Med. 66, 492-497.

Luo, Q., Lu, H., Senseman, D., Worsley, K., Yang, Y., Gao, J.H., 2009. Physiologically evoked neuronal current MRI in a bloodless turtle brain: detectable or not? Neuroimage 47, 1268-1276.

Ogawa, S., Lee, T.M., Kay, A.R., Tank, D.W., 1990. Brain magnetic resonance imaging with contrast dependent on blood oxygenation. Proc. Natl. Acad. Sci. U. S. A. 87, 9868-9872.

Park, T.S., Lee, S.Y., 2007. Effects of neuronal magnetic fields on MRI: numerical analysis with axon and dendrite models. Neuroimage 35, 531-538.

Park, T.S., Lee, S.Y., Park, J.H., Cho, M.H., 2006. Observation of the fast response of a magnetic resonance signal to neuronal activity: a snail ganglia study. Physiol. Meas. 27, 181-190.

Parkes, L.M., de Lange, F.P., Fries, P., Toni, I., Norris, D.G., 2007. Inability to directly detect magnetic field changes associated with neuronal activity. Magn. Reson. Med. 57, 411-416.

Rodionov, R., Siniatchkin, M., Michel, C.M., Liston, A.D., Thornton, R., Guye, M., Carmichael, D.W., Lemieux, L., 2010. Looking for neuronal currents using MRI: an EEG-fMRI investigation of fast MR signal changes time-locked to frequent focal epileptic discharges. Neuroimage 50, 1109-1117.

Singh, M., 1994. Sensitivity of MR phase-shift to detect evoked neuromagnetic fields inside the head. IEEE Trans. Nucl. Sci. 41, 349-351.

Sirotin, Y.B., Das, A., 2009. Anticipatory haemodynamic signals in sensory cortex not predicted by local neuronal activity. Nature 457, 475-479.

Snedecor, G.W., Cochran, W.G., 1989. Statistical Methods (8th ed.). Iowa State University Press, Ames, IA.

Sundaram, P., Wells, W.M., Mulkern, R.V., Bubrick, E.J., Bromfield, E.B., Munch, M., Orbach, D.B., 2010. Fast human brain magnetic resonance responses associated with epileptiform spikes. Magn. Reson. Med. 64, 1728-1738.

Tang, L., Avison, M.J., Gatenby, J.C., Gore, J.C., 2008. Failure to direct detect magnetic field dephasing corresponding to ERP generation. Magn. Reson. Imaging 26, 484-489.

Witzel, T., Lin, F.H., Rosen, B.R., Wald, L.L., 2008. Stimulus-induced Rotary Saturation (SIRS): a potential method for the detection of neuronal currents with MRI. Neuroimage 42, 1357-1365.

Xiong, J., Fox, P.T., Gao, J.H., 2003. Directly mapping magnetic field effects of neuronal activity by magnetic resonance imaging. Hum. Brain Mapp. 20, 41-49.

Xue, Y., Gao, J.H., Xiong, J., 2006. Direct MRI detection of neuronal magnetic fields in the brain: theoretical modeling. Neuroimage 31, 550-559.

APPENDIX

Neural Current Model

We have developed a model for the effect of neuronal currents on the magnetic resonance signal. We have proposed using several different multivariate methods to detect small changes in the magnitude and the phase of a signal. This model can be used to determine the optimal preprocessing methods for neuronal current detection and to determine the location of the neuronal current that might yield the best detection of the signal. The single voxel MR experiment is described in Figure A1D. The radio frequency pulses RF1, RF2, RF3 in the presence of appropriate gradients (not shown in the Figure). The MR signal is measured starting from the center of the echo as indicated in the Figure A1D. It is one-half of the echo and because of its similarity with free-induction decay (FID) signal we also call it FID. Figures A1A to A1C show the neural current response to a stimulus occurring at time 'S'. The neural currents will generate time-varying magnetic field perturbation in the voxel. This time-varying magnetic field perturbation can be described by probability density function $P_{B_n}(B_n(t))$.

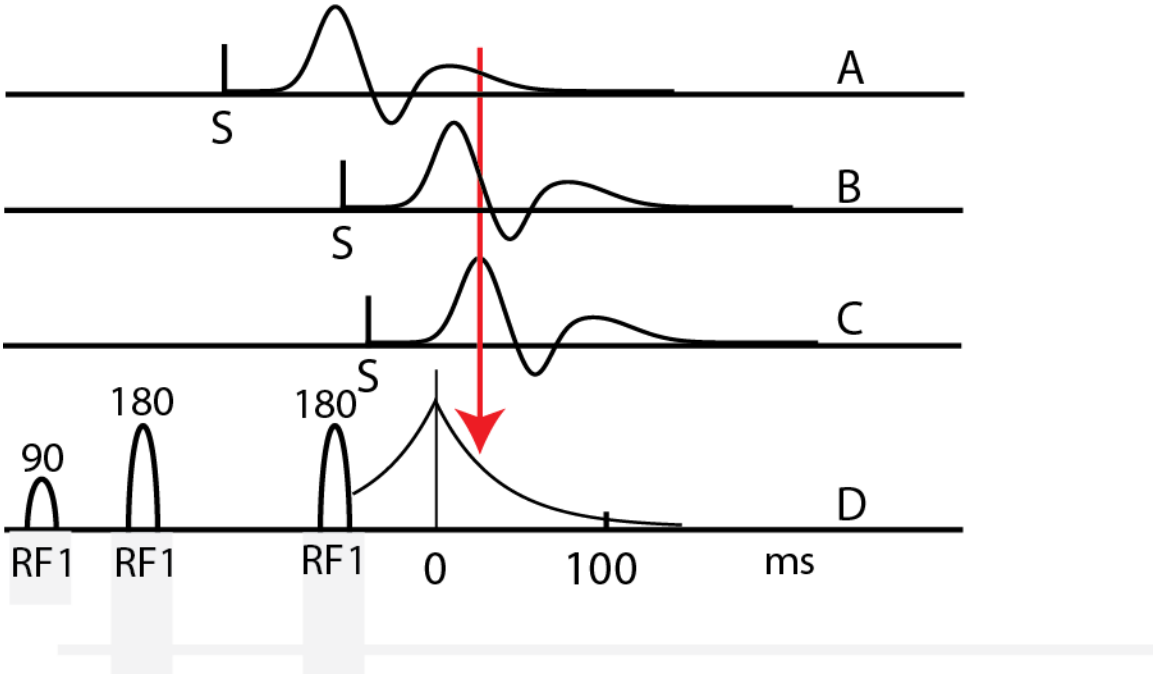

Figure A1: The timing diagram of the MR experiment and its relation to stimulus presentation and the expected neuronal current response

We show that under simplifying assumptions the magnitude of the MR signal depends on the variance of $P_{B_n}(B_n(t))$, and the phase depends on mean of $P_{B_n}(B_n(t))$ (Konn et al., 2003; Marques and Bowtell, 2008). If we assume proton density is uniform in the voxel, then FID can be modeled by

$$S(t) = e^{-R_2^* t} \left\langle e^{-i\phi(r,t)} \right\rangle_V \,, \qquad [1]$$

where the bracket indicates that the average is over the voxel volume and

$$\phi(r,t) = \gamma \int_S^t B_n(r(s),s)ds = \int_S^t \omega_n(r(s),s)ds \,. \qquad [2]$$

In Figures A1A to A1C we show three examples for the start of the stimulus as indicated by 'S' with respect to the MR experiment (Figure A1D). If the neural currents have a response before the 180 rf pulse (Fig. A1A) then Eq.[2] has to be modified to account for the phase reversal caused by the 180 rf pulse. In this study the neural current response was present after the 180 rf pulse only. The results presented here are for the case shown in Figure A1C, where the neural current response begins after we start collecting the data. The results can be modified to cover for case of Figure A1B, where part of the neural current response occurs before the echo-peak.

This average (Eq. [1]) is difficult to compute because $r(t)$ is function of time since spins move because of diffusion. If we assume that spins are stationary, in other words, if we neglect diffusion, then $r(t)$ is not a function of t. With this assumption the volume average in Eq. [1] can be written in terms of $P_{B_n}(B_n(t))$. The MR signal is given by

$$S(t) = e^{-R_2^* t} \int_V e^{-i\gamma \int_S^t B_n(s)ds} P_{B_n}(B_n(t))dB_n \,. \qquad [3]$$

If we further assume that probability distribution $P_{B_n}(B_n(t))$ is not time dependent and is a Cauchy distribution defined by,

$$P_{B_n}(B_n) = \frac{1}{\sqrt{\pi}} \frac{\sigma_{B_n}}{\sigma_{B_n}^2 + (B_n - \mu_{B_n})^2} \,. \qquad [4]$$

then

$$S(t) = e^{-R_2^* t} e^{-i\gamma\mu_{B_n} t} e^{-\gamma\sigma_{B_n} t} \,. \qquad [5]$$

In other words, the magnitude of the MR signal has an additional decay term depending on the standard deviation of $P_{B_n}(B_n)$ and its phase is dependent on the mean of $P_{B_n}(B_n)$ (Marques and Bowtell, 2008).

The neural current response varies during the MR signal. We will model this neuronal current response by the probability distribution function

$$P_{B_n}(B_n(t)) = \frac{1}{\sqrt{\pi}} \frac{\sigma_{B_n}(t)}{\sigma_{B_n}^2(t) + (B_n - \mu_{B_n}(t))^2} \,, \qquad [6]$$

with a time-varying mean and variance. The integral in Eq. [3] is again difficult to calculate, and an approximate solution is given by

$$S(t) = e^{-R_2^* t} e^{-i\phi_n(t)} e^{-R_n(t)}, \qquad [7]$$

where

$$\phi_n(t) = \int_S^t \gamma \mu_{B_n}(s) ds = \int_S^t \omega_n(s) ds, \qquad [8]$$

and

$$R_n(t) = \int_S^t \gamma \sigma_{B_n}(s) ds = \int_S^t \rho_n(s) ds. \qquad [9]$$

A general form for the MR signal with measurement noise and some initial phase is given by,

$$S(t) = e^{-R_2^* t} e^{-i\phi_n(t)} e^{-R_n(t)} e^{-i\phi_0} + \theta(t), \qquad [10]$$

where $R_n(t)$ and $\phi_n(t)$ are changes in decay rate and phase brought about by neural currents. Physiological noise effects will be also appear in these terms and are presently neglected. ϕ_0 is constant for a FID, but it can vary from one FID to another because of a drift in the magnetic field during the course of the experiment. This drift can be caused by heating or other experimental changes. $\theta(t)$ is the additive measurement noise. The signal and the noise are complex. The noise is assumed to be independent in the two channels (real and imaginary) and to have normal distribution. The noise properties should not change from FID to FID unless some external RF interference occurs. The measurement noise includes the instrument noise and the noise generated by the source (subject or an agar phantom). The variance of $\theta(t)$ will be smaller in phantoms than in subjects.

Simulating effects of Neural Currents

The neural current response can be simulated from Eq. [10] if we assume some form for functions $\omega_n(t)$ (Eq. [8]) and $\rho_n(t)$ (Eq. [9]). For purposes of simulation, we will model these by scaled Gaussian functions with some mean and variance. The scaling will modulate the size of the effect, the mean will affect the location (in time) and the variance will influence the duration. Because the cause of the magnitude and the phase change in the signal is the same, we will assume that $\rho_n(t)$ and $\omega_n(t)$ have the same temporal variation. We will choose an arbitrary cut-off of between two standard deviations (σ_R) about the mean (μ_R) to define the duration and the location of the neural current effects. Thus, a model for defining the neural current change is

$$f_n(t) = e^{-\frac{(t-\mu_R)^2}{2\sigma_R^2}} - e^{-2}, \text{ in the interval } [\mu_R - 2\sigma_R, \mu_R + 2\sigma_R]. \qquad [11]$$

$f_n(t)$ is symmetric around μ_R and because we have subtracted the term e^{-2} it goes to zero smoothly outside the range $[\mu_R - 2\sigma_R, \mu_R + 2\sigma_R]$. $f_n(t)$ is scaled to have a maximum value of one.

$\rho_n(t)$ and $\omega_n(t)$ are defined by

$$\rho_n(t) = A_m f_n(t) \qquad [12]$$

and

$$\omega_n(t) = A_\phi f_n(t), \qquad [13]$$

where A_m and A_ϕ are two scaling factors. A_m is chosen to reflect the expected signal percent change and A_ϕ is chosen to reflect the expected phase change.

Let $S_n(t)$ be the signal with the neural current effect and $S_w(t)$ be the signal without the neural current effect. The fractional signal change in the magnitude caused by a change in $\rho_n(t)$ at time T_n is given by,

$$\frac{\Delta S(T_n)}{|S_w(T_n)|} = \frac{|S_n(T_n)| - |S_w(T_n)|}{|S_w(T_n)|} = e^{-\int_S^{T_n} A_m f_n(t)dt} - 1, \qquad [14]$$

which implies

$$A_m = -\frac{\ln(1 + \Delta S(T_n) / |S_w(T_n)|)}{\int_S^{T_n} f_n(t)dt}. \qquad [15]$$

The scaling factor A_m can be calculated from the above equation. The phase change at T_n is given by

$$\phi_n(T_n) = A_\phi \int_S^{T_n} f_n(t)dt, \qquad [16]$$

from which A_ϕ can be calculated to give the expected phase change.

The following table gives the predicted phase change from two papers.

Reference	ΔS	$\Delta\phi$
K. Blagoev et al. Neuroimage, 2007	0.016	1°
L. Heller et al. Human Brain mapping, 2009	$2x10^{-5}$	0.004°

Konn, D., Gowland, P., Bowtell, R., 2003. MRI detection of weak magnetic fields due to an extended current dipole in a conducting sphere: a model for direct detection of neuronal currents in the brain. Magn. Reson. Med. 50, 40-49.

Marques, J.P., Bowtell, R.W., 2008. Using forward calculations of the magnetic field perturbation due to a realistic vascular model to explore the BOLD effect. NMR Biomed. 21, 553-565.

DISTRIBUTION (ALL COPIES ELECTRONIC)

2 Andrew R. Mayer, Arvind Caprihan, Charles Gasparovic
The Mind Research Network
1101 Yale Blvd. NE
Albuquerque, New Mexico 87106

1	MS0829	Edward V. Thomas	00431
1	MS0895	Howland D. T. Jones	08622
1	MS0895	David M. Haaland	08622
1	MS0895	Jason C. Harper	08622
1	MS1327	John S. Wagner	01462
1	MS1413	James P. Carney	08622

1	MS0899	Technical Library	9536
1	MS0359	D. Chavez, LDRD Office	1911


Sandia National Laboratories